Fugtfordeling i absorberende isoleringsmaterialer

Peuhkuri, Ruut; Rode, Carsten; Padfield, Tim; Hansen, Kurt Kielsgaard; Hedegaard, Lone

Publication date:
2003

Document Version
Publisher's PDF, also known as Version of record

BYG•DTU

Ruut Peuhkuri
Carsten Rode
Tim Padfield
Kurt Kielsgaard Hansen
Lone Hedegaard

Fugtfordeling i absorberende isoleringsmaterialer

Moisture distribution in absorbent insulation

DANMARKS
TEKNISKE
UNIVERSITET

Sagsrapport
BYG•DTU SR-03-11
2003
ISSN 1393-402x

FUGTFORDELING I ABSORBERENDE ISOLERINGSMATERIALER

Forord

Den foreliggende rapport udgør rapporteringen for projektet "Fugtfordeling i absorberende isoleringsmaterialer" (ENS j.nr.75664/00-0045) finansieret af Energistyrelsens Udviklingsprogram for miljø- og arbejdsmiljøvenlig isolering. Projektet er gennemført af BYG·DTU med lektor Carsten Rode som projektleder.

Øvrige medvirkende ved projektets gennemførelse har været:

- Ph.d.-studerende, civ.ing. Ruut Peuhkuri, BYG·DTU
- Museumsinspektør Tim Padfield, Nationalmuseet, Bevaringsafdelingen
- Lektor Kurt Kielsgaard Hansen, BYG·DTU

Endelig har civ.ing. Lone Hedegaard bistået ved rapporteringen af projektet.

Projektet har haft to hovedelementer: Etablering af et bredt datagrundlag af fugtmæssige egenskaber for alternativ og konventionelle isoleringsmaterialer under såvel stationære som dynamiske prøvningsbetingelser med en samtidig temperaturforskel over materialet. De dynamiske påvirkninger er døgnperiodiske svingninger, som vil kunne afsløre, om de absorberende materialer opfører sig ikke Fick'sk under cykliske påvirkninger. Nærværende rapport udgør dokumentationen for det udførte arbejde, og er derfor i sagens natur af ret teknisk karakter. Det bredere sigte fremgår overvejende af rapportens indledende afsnit.

Dokumentationen er udformet som en kort og mindre teknisk dansk rapport med et tilhørende engelsk appendiks. Det engelske appendiks indeholder den mere teknisk prægede dokumentation.

Civilingeniør Georg Christensen, Bygge- og Miljøteknik A/S, har beredvilligt kommenteret rapporten og de fremkomne resultater. Endvidere har de anvendte målemetoder og foreløbige resultater været fremlagt ved Nordisk Symposium i Bygningsfysik 2002 (Peuhkuri et al., 2002) og ved et møde i SOFUS-BYGs klimaskærmsgruppe 24.03.2003. Projektgruppen takker for de fremkomne kommentarer!

Lyngby, 30. april 2003
Carsten Rode

Indholdsfortegnelse

Dette er en kortfattet dansk udgave af den engelske rapport ” Moisture distribution in absorbent insulation”, der som Appendiks A indgår som en bestanddel af nærværende rapport. Der henvises til dette appendiks for en mere detaljeret forsøgsbeskrivelse og resultatgennemgang.

1 Baggrund

Den danske byggetradition er ved at ændre sig, således at der i dag bruges flere lette konstruktioner. Det kan give fugtproblemer, hvis dampspærren er defekt eller helt er udeladt. Fugtproblemerne skyldes, at fugtbevægelse sker fra den varme til den kolde side af et materiale, hvilket kan føre til en fugtophobning på den kolde side, som i værste fald kan nedbryde konstruktionen. Derfor er det vigtigt at undersøge, hvordan konstruktionerne kan fugtsikres. Man ved at hygroskopiske materialer som fx papirisolering kan optage mere fugt end ikke hygroskopiske materialer som fx stenuld. Dermed vil hygroskopiske materialer bedre kunne modstå kortere perioder med opfugtning, hvis der efterfølgende sker en udtørring.

Endvidere formodes det, at hygroskopiske materialer er i stand til at sende vand retur til den varme side af materialet. Temperaturgradientens indflydelse på denne resulterende fugttransport gennem klimaskærmen er et spørgsmål som med jævne mellemrum er oppe til debat. For nylig har introduktionen af såkaldt "alternative" isoleringsmaterialer – hovedsagligt organiske produkter, som også er meget hygroskopiske – ledt til en debat i Danmark om, hvorvidt der i disse materialer eksisterer ”andre” fugttransportformer, end den som er umiddelbart forklarlig ud fra gradienter i damptrykket. En sådan ”anden” transport er interessant, fordi den måske kunne være med til at sikre konstruktioner mod skadelige fugtpåvirkninger.

1.1 Stationære forhold

Som tidligere nævnt, sker fugtbevægelse normalt fra den varme til den kolde side af et materiale, hvilket kan føre til en fugtophobning på den kolde side, hvis konstruktionen er udført uhensigtsmæssigt. Imidlertid sker denne ophobning tilsyneladende ikke altid for nogle af de organiske materialer. I den forbindelse er det uafklarede spørgsmål; hvilken mekanisme driver den ”anden” transportform, som leder vandet væk fra den kolde side og kan denne kvantificeres. Under stationære forhold kan en fugtstrømning, foruden af damptrykket, forårsages af forskelle i temperatur, vandindhold, kapillartryk eller relativ fugtighed.

I de fleste beregningsmodeller tages der ikke højde for den mulige ”anden” transportform gennem porøse absorberende materialer, som er påvirket af både en termisk og en relativ fugtighedsgradient. De primære drivende potentialer kan virke i samme retning, hvilket gør det meget svært at identificere de enkelte bidrag.

1.2 Dynamiske forhold

Ved dynamiske simuleringer regnes der med, at der opnås lokal hygrotermisk ligevægt i små delområder af materialet. Denne tilnærmelse er almindeligt brugt, da den lille fejl, det forårsager, ofte kan negligeres. Det er muligvis ikke tilfældet, når der er tale om materialer med forsinket sorption (ikke-Fick'sk transport). Det centrale problem med simuleringsmodeller er konflikten mellem, at materialeparametrene er angivet for stationære tilfælde, mens randpåvirkningerne er dynamiske.

2 Formål

Det er målet med projektet at gennemføre en forsøgsrække, der kan bruges til at bestemme de dynamiske fugtbevægelser i materialer, som er udsat for samtidige fugt- og temperaturgradienter. Under disse forhold studeres den resulterende fugttransport og -fordeling indhold i materialet.

Resultaterne skulle gerne føre til erkendelse af, hvordan de undersøgte materialer opfører sig med hensyn til to egenskaber:

1. Det ønskes undersøgt i hvilket omfang, der i materialerne finder en supplerende fugttransport sted end den, som umiddelbart kan forklares ved gradienter i damptryk, fx som en transport fra kold mod varm side af et prøvelegeme, eller fra høj mod lav relativ fugtighed.
2. Det ønskes endvidere at undersøge, om materialerne opfører sig "ikke-Fick'sk" under dynamiske påvirkninger. Dette skulle betyde, at den konventionelle teori for instationære fugtberegninger ikke holder, idet det skulle indebære, at materialerne på en ikke nøjere erkendt måde har en særlig egenskab til at begrænse udsving i fugtindhold.

Alle undersøgelser foregår i det hygroskopiske område - det vil sige med relative fugtigheder på ikke over 95%.

3 Eksperimenter

Et specielt klimakammer, kaldet ”megakoppen” er blevet opbygget i et tidligere projekt. Megakoppen er detaljeret beskrevet i Padfield et al. 2001 og Padfield et al., 2002..

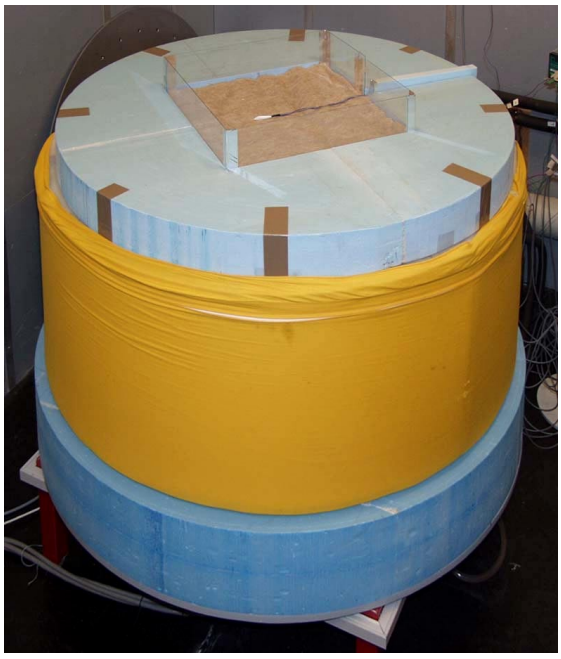

Figur 1A: Billede af megakoppen i funktion. Den kvadratiske materialeprøve ses øverst midt i feltet af cirkulær randisolering.

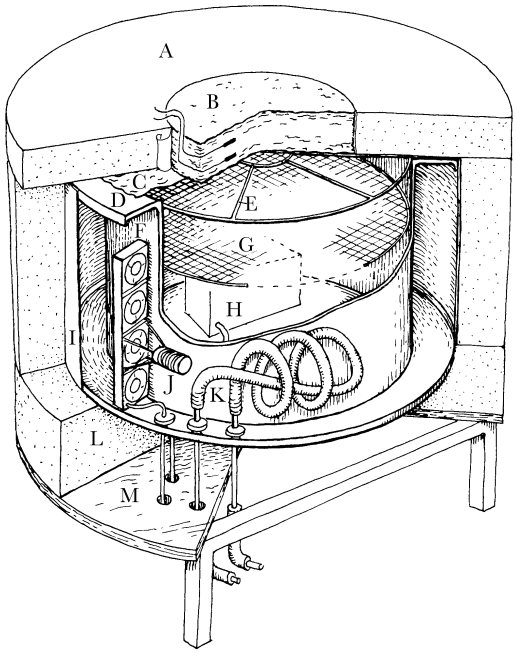

Figur 1B: Principskitse af kammeret til måling af vanddampstrøm gennem et prøveemne med samtidig fugt- og temperaturgradient. Inde i kammeret er der altid køligere end i det omgivende rum. Bevægelsen af vand og vanddamp gennem prøveemnet måles ved at veje vandet som afgives eller absorberes i kammerets klimaanlæg.

Alle forsøgene er udført i megakoppen, som er vist i figur 1A og B. Det specielle ved megakoppen er muligheden for at måle fugtstrømmen enten til eller fra luften i megakoppens kammer. Det gøres ved enten at fordampe eller fortætte vand i et lille vandkar inde i kammeret, som vejes kontinuerligt. Da kammeret ikke selv ophober vand af betydning, indikerer vægtændringen samtidig retningen og størrelsen af fugtstrømmen gennem prøveemnet.

Et af hovedformålene med denne undersøgelse er at studere den lokale fugtfordeling i materialeprøver, som er udsat for en temperaturgradient. Derfor er der placeret små temperaturfølere (termoelementer, type K) og relativ fugtighedsmålere (Honeywell, type HIH-3605-B) jævnt igennem tykkelsen af materialet. For at mindske usikkerhederne, som er forbundet med randeffekterne, måles såvel de relative fugtigheder som temperaturen også på materialeoverfladerne. Placeringen af følerne kan ses af figur 2.

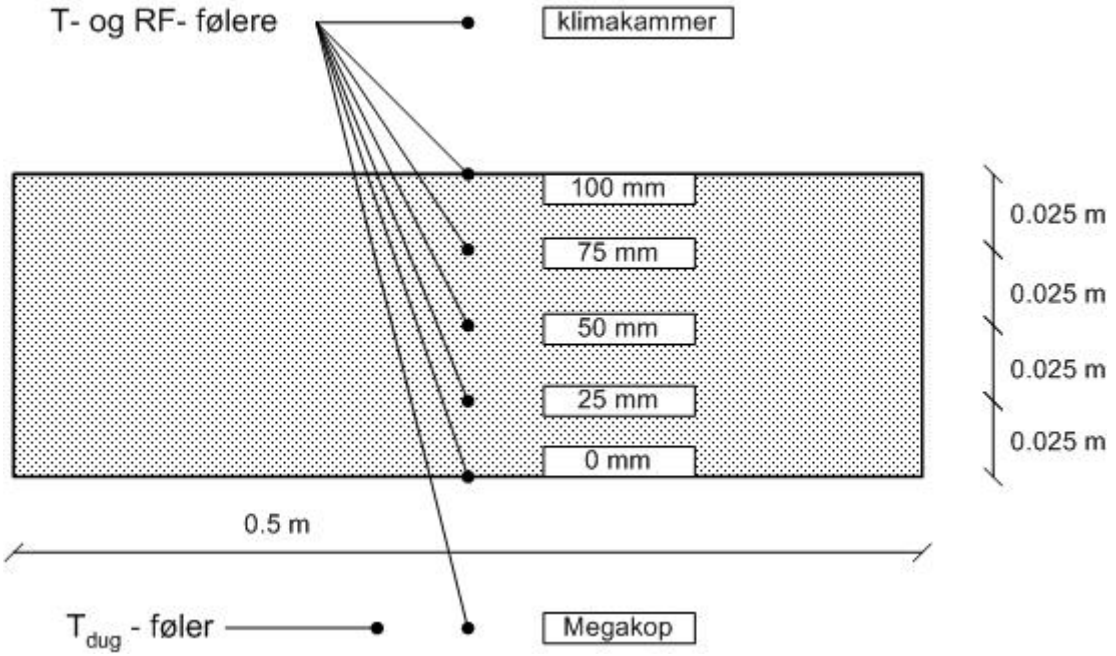

Figur 2: Skitse af temperatur- og relativ fugtighedsfølernes placering gennem materialeprøven. Dybden af placeringens regnes konsekvent nede fra megakoppen ud til klimakammeret. Også placering a. T_{dug} - føler ses.

3.1 Materialer

For at udføre ikke-isoterme eksperimenter skal der opretholdes en temperaturgradient over materialet. Det er derfor en fordel, at eksperimenterne er udført med termiske isoleringsmaterialer. Desuden er materialerne valgt ud fra en antagelse om, at nogle af dem vil udvise en fugttransport drevet af andet end damptryksgradienten, mens andre ikke vil. Desuden forventes forskellige reaktioner når materialerne udsættes for dynamiske fugtpåvirkninger. De valgte materialer er primært alternative isoleringsmaterialer, men til sammenligning er der også medtaget traditionelle isoleringsmaterialer. Derfor er de undersøgte materialer: Papirisolering, fåreuld, hør og stenuld, glasuld, porebeton og ekspanderet perlite. I tabel 1 ses materialeparametrene og dimensionerne af de testede prøveemner.

Materiale	Tørdensitet ρ_d [kg/m^3]	Varmeledningsevne λ [W/m·K]	Prøvetykkelse d [mm]
Papirisolering, løsfyld	65	0,040	100
Fåreuld	25	0,039	100
Hør	30	0,040	90
Stenuld	30	0,039	100
Glasuld	70	0,039	100
Porebeton	450	0,11	100
Perlite, løsfyld	100	0,050	100/140

Tabel 1: Materialeparametre for materialer brugt til ikke isoterme forsøg. Materialeparametrene for papirisolering, fåreuld, hør, stenuld og perlite stammer fra (Hansen m.fl., 1999) Tørdensiteten for glasuld, porebeton og perlite er bestemt som en del af dette arbejde. Varmeledningsevnen for porebeton er bestemt i et studenterprojekt (Delfino and Giacchetti, 2001). Forsøgene med perlite er udført med to prøvetykkelser.

3.2 Beskrivelse af eksperimenter

Der er udført to serier af eksperimenter: En serie stationære målinger og en serie dynamiske målinger. Den stationære serie består af fire tilfælde.

1. Ingen fugttransport: Gradienterne i temperatur (T) og relativ fugtighed (RF) er modsatrettede og der vil ikke være nogen damptryks-gradient (p), hvis fugttransporten udelukkende drives af damptrykket.
2. Konstant RF: T- og p-gradienterne er ensrettede og der er ingen RF-gradient.
3. Modsatte potentialer: p- og RF-gradienterne er modsatrettede, og T-gradienten er i samme retning som p-gradienten.
4. Parallelle potentialer: p- og RF-gradienterne er parallelle i samme retning og T-gradienten er modsat de andre gradienter.

I figur 3 ses en principiel skitse af de fire forskellige ikke isoterme stationære tilfælde, og til sammenligning er der medtaget et eksempel på et almindeligt isotermt kopforsøg.

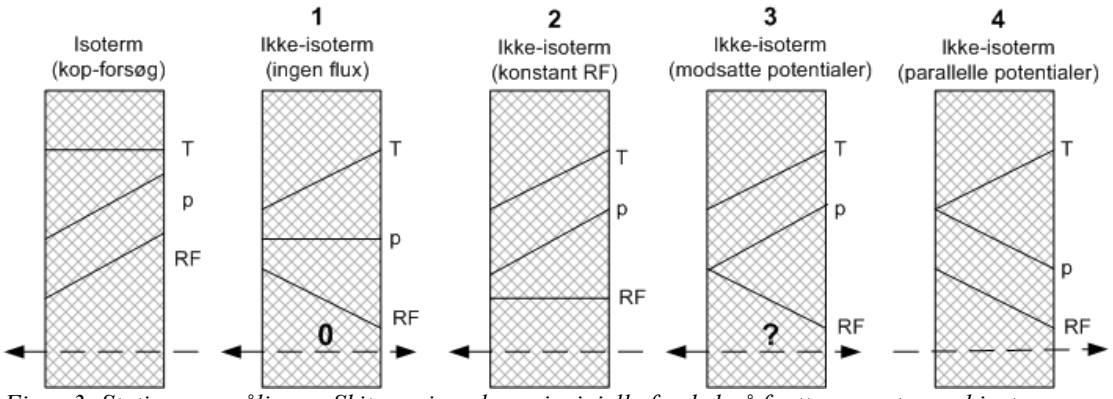

Figur 3: Stationære målinger. Skitsen viser den principielle forskel på fugttransporten ved isoterme og ikke isoterme kopforsøg. Desuden ses gradienternes principielle retning for de 4 forsøgstilfælde.
T er temperaturen, p er damptrykket og RF er den relative fugtighed.

Den dynamiske serie består af to tilfælde. Fugtvariation følger i begge tilfælde en sinuskurve, som kan ses i figur 4.

1. Fugtvariationen varierer døgnperiodisk i intervallet 65% < RF < 85%
2. Fugtvariationen varierer døgnperiodisk i intervallet 75% < RF < 95%

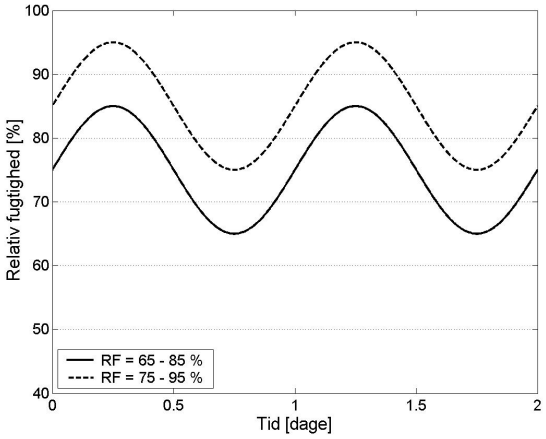

Figur 4: Dynamiske målinger. Sinusvariationen i den relative fugtighed inde i megakoppen. De to forskellige fugtniveauer er begge afbilledet.

4 Resultater

4.1 Stationære forhold

Hvis det først antages, at damptrykket er det eneste drivende potentiale kan en tilsyneladende damppermeabilitet, δ_p beregnes. Det gøres ved brug af følgende formel:

$$\delta_p = g \cdot \frac{d}{\Delta p},$$

hvor
g er fugtstrømmen [kg/(m^2·s)]
d er materialetykkelsen [m]
Δp er damptryksforskellen [Pa]

Beregningen af tilsyneladende permeabilitet for prøvematerialerne kan ses i tabel 2.

Materiale	Isoterm permeabilitet δ_p $\cdot 10^{-9}$ [kg/(Pa·m·s)]	Tilsyneladende permeabilitet		
		$\delta_{p,RH}$ (tilfælde 2) $\cdot 10^{-9}$ [kg/(Pa·m·s)]	$\delta_{p,mods}$ (tilfælde 3) $\cdot 10^{-9}$ [kg/(Pa·m·s)]	$\delta_{p,par}$ (tilfælde 4) $\cdot 10^{-9}$ [kg/(Pa·m·s)]
Papirisolering	0,110 ± 0,002	0,13	0,12	0,50 - 1,0
Fåreuld	0,190 ± 0,052	-	0,14	0,35
Hør	0,150 ± 0,059	-	0,083 - 0,14	0,37
Stenuld	0,183 ± 0,03	0,19	0,17 - 0,21	0,39 - 0,48
Glasuld	0,170 ± 0,01	-	0,15	0,44
Porebeton	0,024 ± 0,0004	-	0,023 - 0,045	0,19
Perlite	0,103 ± 0,015	0,093	0,068 - 0,072	-

Tabel 2: Isoterme vanddamppermeabiliteter for de undersøgte materialer. Nogle er bestemt som en del af dette arbejde og resten stammer fra (Hansen et al., 1999). Herudover indeholder tabellen beregnede tilsyneladende damppermeabiliteter udfra ikke isoterme måleresultater i Megakoppen, hvor det er antaget at damptrykket er det eneste drivende potentiale.

Af tabel 2 fremgår det, at den isoterme damppermeabilitet for stenuld er næsten identisk med den beregnede for tilfælde 2, hvor den relative fugtighed holdes konstant. Under isoterme forhold går damptryk- og relativ fugtighedsgradienten i samme retning, og en evt. ”anden” transport er parallel med dampdiffusionen. Ligeledes gælder, når den relative fugtighed er konstant, så går temperatur- og damptryksgradienten i samme retning, og derfor er det svært at konkludere, hvilket potentiale der driver den ”anden” transport.

Tilfælde 3 udviser i flere tilfælde den mindste permeabilitet. Da der er ensrettede gradienter for temperaturen og trykket, og en modsatrettet gradient for relativ fugtighed, kunne det betyde, at den relative fugtighed giver anledning til en ”anden” transport.

I tilfælde 4 hvor den relative fugtighed og damptrykket er parallelle potentialer, er permeabiliteten højere end i alle øvrige tilfælde. Det er en klar indikation af, at der er en ”anden” transport, som forstærkes af, at gradienten i relative fugtighed nu trækker transporten i samme retning som damptrykket.

At permeabiliteten tilsyneladende forøges når potentialerne for damptrykket og den relative fugtighed er parallelle fremgår ligeledes af figur 5. Her, som i de følgende grafer illustreres resultaterne kun for papirisolering og stenuld, mens tabellerne viser de talmæssige resultater for alle materialer.

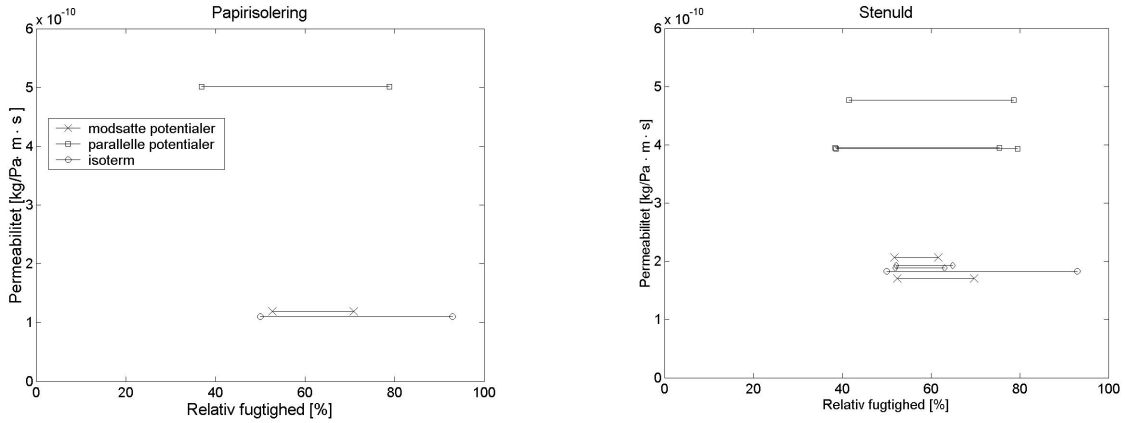

Figur 5: Målte isoterme (o) og tilsyneladende vanddamppermeabiliteter for papirisolering og stenuld. Randpåvirkningerne er; konstant RF (tilfælde 2) kun for stenuld (◇), modsatte potentialer (tilfælde 3)(×) og parallelle potentialer (tilfælde 4) (□).

For yderligere at illustrere, at der findes en ”anden” transport, er der lavet en figur, der viser fugtstrømmen g som en funktion af damptryksforskellen over materialet. Dette ses i figur 6.

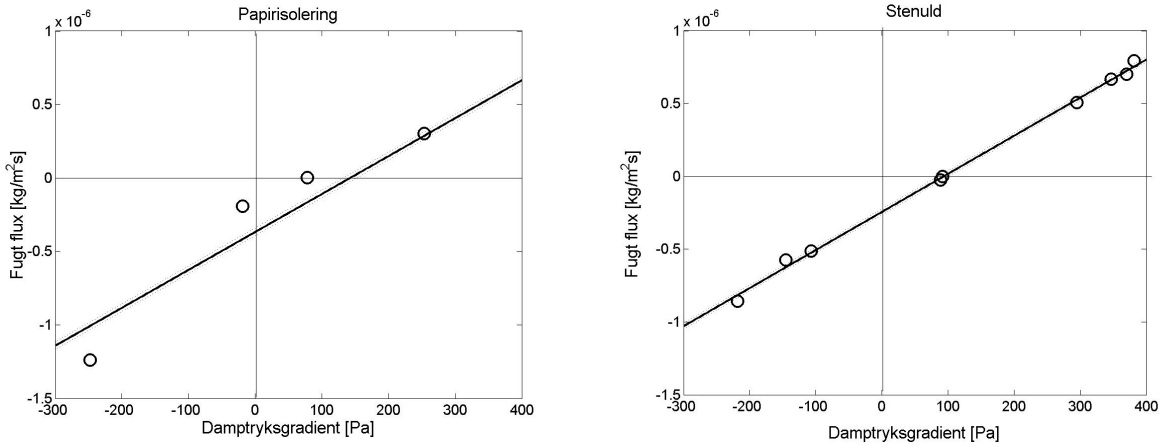

Figur 6: Fugtstrøm (g) som en funktion af damptryksforskellen (Δp) for papirisolering og stenuld.

Af figur 6 ses, at der ikke er skæring med y-aksen gennem (0,0), hvilket skulle være tilfældet, hvis Δp var det eneste drivende potentiale. Skæringen med y-aksen indikerer derfor størrelsen af den "anden" transport.

Størrelserne af den "anden" transport fremgår af tabel 3.

Materiale	"Anden" transport [kg/m^2·s]
Papirisolering	$3{,}7 \cdot 10^{-7}$
Fåreuld	-
Hør	$0{,}45 \cdot 10^{-7}$
Stenuld	$2{,}4 \cdot 10^{-7}$
Glasuld	$1{,}6 \cdot 10^{-7}$
Porebeton	$1{,}5 \cdot 10^{-7}$
Perlite	$1{,}2 \cdot 10^{-7}$

Tabel 3: Størrelsen af fugttransporten i modsat retning af damptryksgradienten for de undersøgte materialer. Den anden transport er fundet som skæringen med y-aksen i figur 6.

Af tabellen fremgår det, at den "anden" transport måske er størst for papirisolering, men også materialerne stenuld, glasuld, porebeton og perlite har en signifikant "anden" transport modsatrettet damptryksgradienten, mens signifikansen for hør er lille.

For tilfælde 1 er det tilstræbt at der ikke er nogen fugtstrøm gennem materialet. Hvis der ikke var "anden" fugttransport end den forårsaget af damptrykket, ville damptrykket være på samme niveau i megakoppen og i klimakammeret, og ud fra denne antagelse vil man kunne beregne en teoretisk værdi af de relative fugtigheder i megakoppen.

	Relativ fugtighed i megakoppen		
	Målte værdier		Teoretiske værdier
Materiale	RF – føler *[% RF]*	T_{dug} – føler *[% RF]*	Δp = 0 *[% RF]*
Papirisolering	80	87	88
Fåreuld	-	-	-
Hør	93	95	97
Stenuld	81	89	88
Glasuld	81	89	88
Porebeton	87	90	94
Perlite	76	79	84

Tabel 4: Sammenstilling af målte og teoretisk beregnede værdier for den relative fugtighed i megakoppen, når der ikke er nogen fugtstrøm (tilfælde 1), hvilket gælder hvis det eneste drivende potentiale er damptryksforskel, Δp. T_{dug} er en dugpunktsmåler og T_{dug} er omregnet til relativ fugtighed. Forskellen mellem de 2 RF-følere er forklaret i den efterfølgende tekst.

Af tabellen fremgår det, at i henhold til RF-føleren er den resulterende relative fugtighed i megakoppen lavere for alle materialer. Det kunne betyde, at der er en fugttransport modsat damptryksgradienten, som medfører, at den relative fugtighed på den kolde side af materialet (12 °C) bliver mindre end forventet. Derfor vil materialet være bedre i stand til at beskytte sig selv mod for høje relative fugtigheder. Det er overraskende, at den samme effekt også kan ses for ikke hygroskopiske materialer som perlite, mens effekten er mindre for hør, som ellers er meget hygroskopisk.

Det er desværre også sådan, at den registrerede forskel mellem teoretiske og målte relative fugtigheder er af samme størrelsesorden som usikkerheden på de små relativ fugtighedsfølere. Til sammenligning er der i megakoppen ligeledes målt relativ fugtighed med en dugpunktsmåler (mærke: Campbell Scientific). Resultaterne heraf ses i anden talkolonne i

tabel 4. Usikkerheden fremgår af den store forskel mellem de 2 forskellige føleres målte relative fugtigheder i megakoppen. Ud fra resultaterne kan det derfor ikke konkluderes, at den resulterende RF i megakoppen bliver mindre for nogen af materialerne end den teoretiske RF.

4.2 Dynamiske forhold

Figur 7 viser udviklingen i relativ fugtighed ind gennem to af materialerne over en periode på 48 timer, når den relative fugtighed svinger med en sinusvariation mellem 65 og 85 % RF.

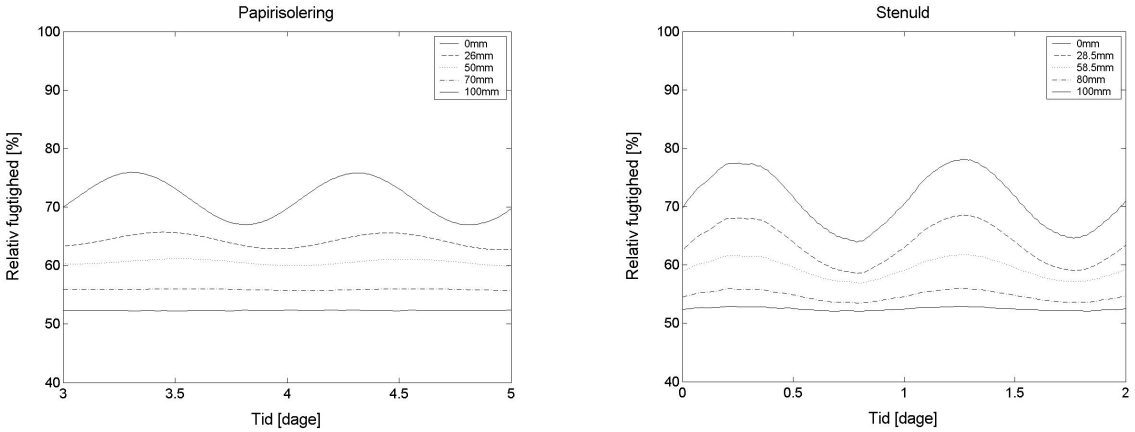

Figur 7: Den målte fordeling i relativ fugtighed gennem materialet for papirisolering og stenuld, når randbetingelserne er en sinusvariation mellem 65 – 85 % RF inde i megakoppen. Afstanden i materialet er angivet inde fra megakoppen.

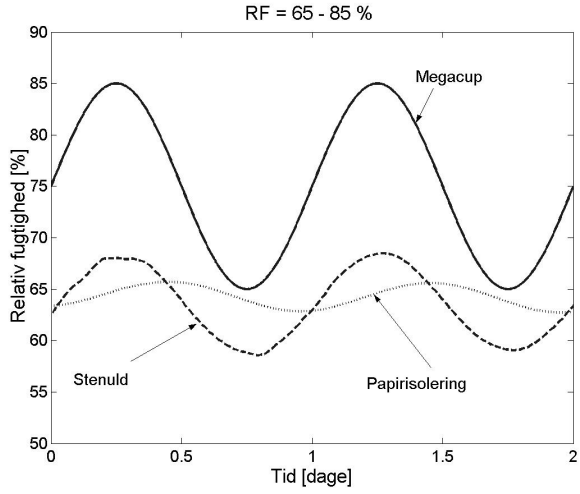

Figur 8: Målt relativ fugtighed i ca. samme dybde af prøvematerialet. Måledybden af papirisoleringen er 26 mm, og for stenuld er den 28,5 mm indefra megakoppen. Megakoppens sinusvariation er fra 65 – 85 % RF.

Figur 8 viser ligesom figur 7 den målte relative fugtighed, men her sammenlignes variationen i 2 materialer i næsten samme dybde. Når man ser nærmere på figur 8, er det klart, at der er to hovedobservationer:

1. Der er meget mindre variation i den relative fugtighed for papirisoleringen end for stenulden. Dette indikerer, at fugtbufferkapaciteten er størst for papirisoleringen.

2. Det kan bemærkes at papirisoleringen har en stor faseforskydning (forsinkelse af toppunktet i materialet i forhold til sinuspåvirkningen), mens stenuld kun har en lille forsinkelse.

Faseforskydningen forøges med dybden for alle materialer.

Den 1. hovedobservation indikerer en fugtbufferkapacitet, og for at beskrive denne er det nødvendigt at indføre begrebet indtrængningsdybde. En indtrængningsdybde kan defineres som den dybde fra overfladen af materialet, hvor påvirkningen på overfladen er reduceret til 36,7 %. Denne definition er brugt i det følgende.

Reelt angiver en indtrængningsdybde hermed det aktive lag af materialet, hvor fugt kan optages eller afgives. Omvendt er den inaktive del af et materiale udsat for en næsten stationær tilstand hvad angår fugtoptag og –afgivelse.

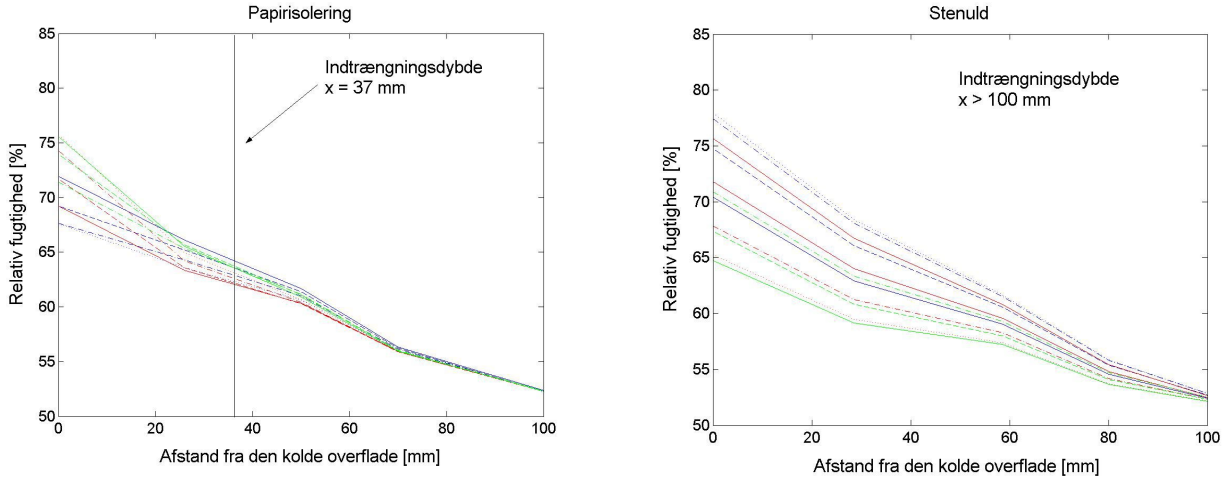

Figur 9: Viser de målte fugtvariationer ind gennem materialerne: Papirisolering og stenuld. Desuden er den målte indtrængningsdybde markeret.

I figur 9 ses den indtrængningsdybde, som er bestemt ved brug af relativ fugtigheds-målingerne i materialerne. Indtrængningsdybderne er fundet for alle de testede materialer, hvilket fremgår af tabel 5.

Materiale	Indtrængningsdybde *[mm]*
Papirisolering	37
Fåreuld	~100
Hør	35
Stenuld	>100
Glasuld	55
Porebeton	32
Perlite	85

Tabel 5: Målte indtrængningsdybder for ikke-isoterme sinusvariationer i megakoppen. Tallene er fremkommet ved at sammenholde den målte fugtfordeling i materialet med den teoretiske model for fugtfordeling i materialer for RF=65-85%..

Af tabellen ses det, at indtrængningsdybden er størst for materialerne perlite, glasuld og stenuld, mens papirisolering, hør og porebeton har de mindste indtrængningsdybder. For stenuld er indtrængningsdybden større end materialetykkelsen (100 mm).

Indtrængningsdybden alene fortæller ikke i sig selv noget om et materiales fugtbufferevne. Der er indført nogle begreber, der bedre beskriver materialers evne til at udjævne udsvingninger i omgivelsernes relative luftfugtighed. En af disse er $\Delta m_{w,}$ der angiver mængden af vand, der kan flyttes til og fra materialet for en given ændring i omgivende

relativ fugtighed med en given periodisk udsving. Denne værdi er vist i tabel 6, hvor det også kan ses, at papirisolering sammen med fåreuld og porebeton udviser en god bufferevne. Derimod har stenuld og perlite ikke nogen bufferevne af betydning.

Materiale	Tilgængelig vand Δm_w *[g/(m² 10%RH 24 h)]*
Papirisolering	78
Fåreuld	71
Hør	48
Stenuld	11
Glasuld	22
Porebeton	65
Perlite	7

Tabel 6: Δm_w for ikke isoterme sinusvariationer (65–85%) i megakoppen med en periode på 24 timer og ændring i relativ fugtighed på 10 %RF. Den målte indtrængningsdybde indgår i beregningen.

4.3 Simuleringer

Der er lavet en sammenligning mellem måleresultater og resultater fra en numerisk simulering. Simuleringsmodellen er baseret på de samme partielle differentialligninger og materialeparametre som programmet MATCH (Rode, 1991), og er detaljeret beskrevet i (Peuhkuri, 2002). Den benyttede model benytter sig ikke af hysterese, men bruger en gennemsnitlig sorptionskurve. Betydningen af hysteresen er studeret for et enkelt materiale.

Ved simuleringerne er de aktuelle målte relative fugtigheder indsat som randbetingelser. Resultaterne af simuleringerne kan ses af figur 10.

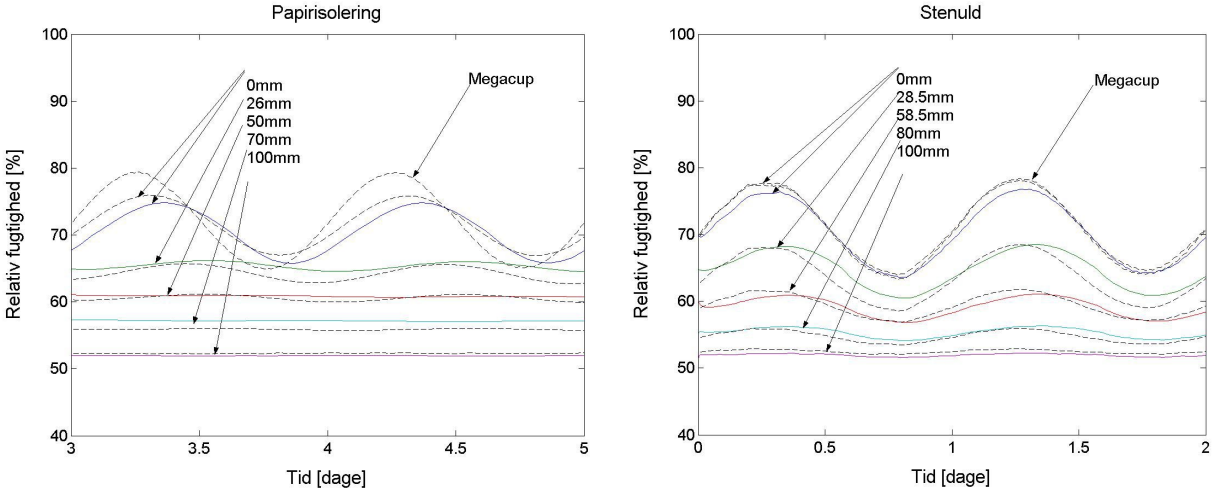

Figur 10: Sammenligning af målte og simulerede relative fugtighedsfordelinger ind gennem materialet. De dynamiske randbetingelser inde i megakoppen er givet ved en sinuskurve, der varierer mellem 65 og 85 % RF. De målte værdier er angivet med stiplede linier, og de simulerede med fuldt optrukne linier.

Af figuren fremgår det, at der er god overensstemmelse mellem de målte resultater og simuleringerne for papirisolering og stenuld. Dette gælder også for hør og perlite. Yderligere viser simuleringerne en lille faseforskydning for alle materialer. Det kunne indikere, at materialerne ved de dynamiske prøvningsbetingelser har en mindre fugtkapacitet end den, der er bestemt ud fra sorptionsisotermens hældning, som benyttes af modellen. Den største afvigelse mellem de eksperimentelle målinger og simuleringerne blev set for porebeton, hvor den simulerede variation i relativ fugtighed fluktuerer meget mindre end målingerne.

Modellering med hysterese, hvilket i sig selv fører til en mindre fugtkapacitet, fjernede faseforskydningen men gjorde samtidig udsvingningerne i RF lidt større. Hovedobservationen er, at fugtkapaciteten tilsyneladende er mindre and givet ved sorptionsisotermer, og permeabiliteten er en smule større end data fra de stationære målinger indikerer.

En mulig forklaring på afvigelserne kan også være brugen af relativ fugtighedssensorerne og antagelsen om lokale ligevægtstilstande mellem den absorberede fugt og luftfugtigheden i simuleringsmodellen. Det reelle fugtindhold i et materiale afhænger ikke nødvendigvis af den målte relative fugtighed, men det gør den i modellen. Derfor kan ændringerne i den målte relative fugtighed variere en smule hurtigere end det tilsvarende fugtindhold i materialet.

5 Konklusion

Resultater af målinger af fugttransport og -fordeling i de undersøgte alternative og traditionelle isoleringsmaterialer tyder på, at der finder en anden transport sted end den, der alene drives af damptryksforskelle. Resultaterne kan dog ikke umiddelbart understøtte en opfattelse om, at hygroskopiske isoleringsmaterialer, såsom papirisolering, har en særskilt egenskab, der beskytter materialet mod for store fugtophobninger på den kolde side af isoleringen. Det ser nemlig ud til, at alle de undersøgte isoleringsmaterialer, både de ikke-hygroskopiske, som fx stenuld, og de hygroskopiske, udviser samme principielle egenskaber for fugttransport.

Beklageligvis må det dog erkendes, at nogle af de gennemførte målinger formentlig ikke har været tilstrækkelig nøjagtige til, at man kan drage særlig vidtrækkende konklusioner ud fra prøvningsresultaterne. Ikke desto mindre synes der dog at have tegnet sig nogle tendenser, som her ridses op:

De mest hygroskopiske materialer var bedre i stand til begrænse udsving i den relative fugtighed (RF), end det var tilfældet for de ikke-hygroskopiske. De begrænsede RF-udsving betyder bl.a., at spidsværdierne med høje fugtigheder bliver mindre. Konstruktioner med materialerne porebeton, hør og papirisolering er derfor bedre til at begrænse forekomsten af korte perioder med meget høje fugtigheder, end fx konstruktioner med stenuld, glasuld og perlite. For eksempel er den højeste relative fugtighed i en position 28 mm fra den kolde side op til 5% RF lavere for en konstruktion af porebeton, og op til 7-8% RF lavere for en konstruktion med papirisolering, end de tilsvarende spidsværdier i en konstruktion isoleret med perlite eller glasuld. Forskellen mellem materialerne udviser dog ikke nogen overbevisende entydighed, når måleusikkerheden i de små RF-følere tages i betragtning.

Materialernes fugtbufferevne blev bestemt udfra de dynamiske målinger: Papirisolering har den bedste bufferevne, efterfulgt af fåreuld , porebeton og hør. Glasuld, stenuld og perlite har ikke nogen bufferevne.

En sammenligning mellem målte og beregnede resultater viser, at der for de fleste materialer kan ses en god overensstemmelse med den benyttede beregningsmodel, der anvender konventionel teori for dampdiffusion efter Ficks lov under instationære betingelser. En mindre faseforsinkelse af de beregnede resultater kunne tyde på, at den virkelige fugtkapacitet af materialerne er mindre end den, beregningsmodellens matematik forudsiger. Dette kunne indikere, at det ved de dynamiske forhold, der hersker i praksis, ikke er muligt at udnytte hele den fugtkapacitet, som repræsenteres ved materialernes sorptionskurver. Ved at anvende en

beregningsmodel, der tager hensyn til sorptionshysteresen kan man opnå en bedre overensstemmelse mellem målinger og beregninger.

6 Referencer

Padfield, T., C. Rode, A. Nicolajsen & K. K. Hansen. 2001. "Udstyr til undersøgelse af fugtfordeling i absorberende isolering". Sagsrapport SR-0028, IBE, DTU, 2. udgave, december 2001. http://www.ens.dk/graphics/isolering/99-13.pdf

Padfield, T., R. Peuhkuri, C. Rode & K.K. Hansen. 2002. "Non-Isothermal Water Vapour Transmission through Porous Insulation. Part 1: The Climate Chamber". 6th Symposium on Building Physics in the Nordic Countries. Department of Building and Construction Engineering, NTNU, Trondheim, Norway. http://www.ivt.ntnu.no/bat/bm/buildphys/proceedings/96_Padfield.pdf

Peuhkuri, R., T. Padfield, T., C. Rode & K. K. Hansen. 2002. "Non-Isothermal Water Vapour Transmission through Porous Insulation. Part 2: Measurements". 6th Symposium on Building Physics in the Nordic Countries. Department of Building and Construction Engineering, NTNU, Trondheim, Norway. http://www.ivt.ntnu.no/bat/bm/buildphys/proceedings/95_Peuhkuri.pdf

Peuhkuri, R. 2002. "Simulink model of coupled heat and moisture transport in material layers". Report SR-02-02. Department of Civil Engineering, Technical University of Denmark.

Rode, C. 1991. "Description of the model MATCH. Theoretical background, equations". IEA ECBCS, Annex 24, Report T1-DK-91/01. Thermal Insulation Laboratory, Technical University of Denmark.

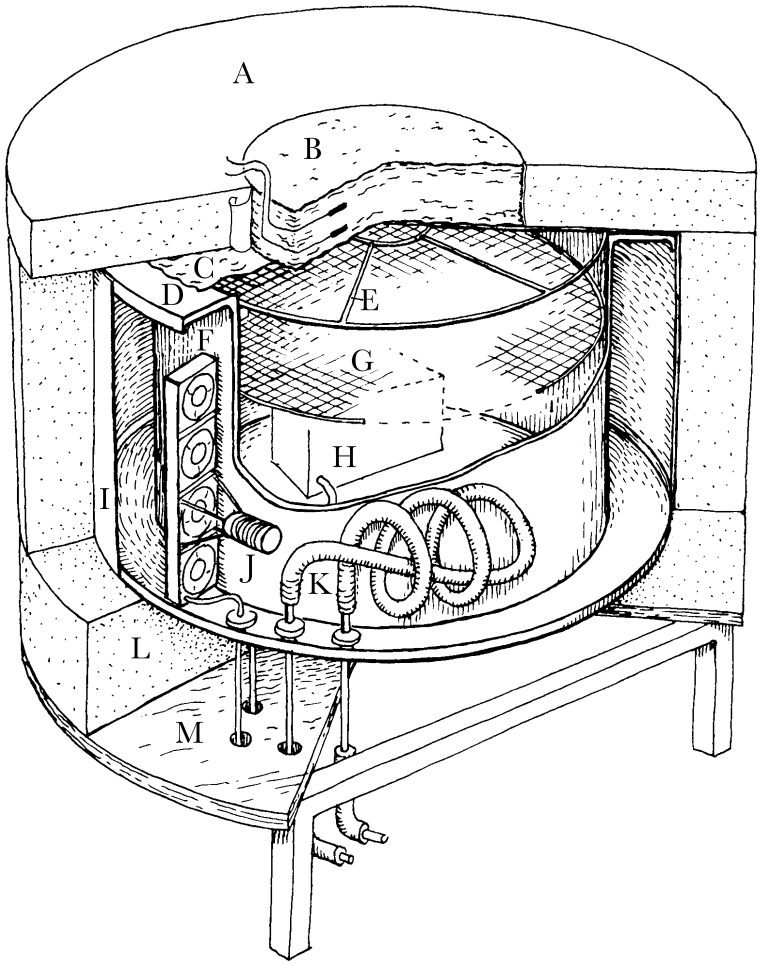

Appendix A
Moisture distribution in absorbent insulation

Ruut Peuhkuri, Carsten Rode, Kurt Kielsgaard Hansen and Tim Padfield
Department of Civil Engineering
Technical University of Denmark

Report to Danish Energy Agency
May 1, 2003

Contents

Chapter 1

Background

The question of the significance of the impact of temperature gradients on the resulting moisture transport in building envelopes is raised every now and then. Recently, the introduction of some 'new' insulation materials – that mostly are of organic origin – has initiated the discussion, at least in Denmark, on the existence, even in the hygroscopic range, of any 'other transport processes' than water vapour pressure driven transport.

1.1 Steady state boundary conditions

Moisture flux can exist – besides that caused by the water vapour pressure gradient – due to a temperature, a moisture content and/or a capillary pressure gradient. The question is: Is this 'other' moisture flux induced by the thermal gradient, by the suction pressure gradient or by the moisture content gradient – and subsequently by the relative humidity gradient, or even by them all. The direction of the moisture content gradient is usually from cold to warm in building envelopes. The direction of the thermal diffusion is theoretically also from cold to warm. These driving potentials can work in the same direction and the identification of the single contributions is very complex.

However, in many simulation models, this possible 'other' movement of moisture through a porous, water absorbent material exposed to both a temperature and a relative humidity gradient is not taken into account. Nevertheless, the assumption of water vapour pressure difference being the only driving force cannot be entirely correct, because this process will result in a gradient of absorbed moisture content within the material, which will then tend to drive water in the opposite direction even in the hygroscopic range (Padfield, 1999). Deviations between simulations and measurements reported in e.g. (Peuhkuri, 2000) for cellulose insulation, which is a very hygroscopic material, could be an indication of these phenomena.

The methods and results in (Kumaran, 1988), (Krus, 1995) and (Galbraith et al., 1998; Galbraith et al., 1999; Galbraith et al., 2000) have in many ways given the background and inspiration to the present analysis. Some of their conclusions are included here:

The conclusion in (Kumaran, 1988) was – based on the resulting moisture profile – that for cellulose insulation there exists a liquid phase transport against the water vapour gradient. Under the observed final steady state conditions this liquid transport is of same magnitude as the transport driven by the water vapour pressure gradient, because the net transport was zero.

(Krus, 1995) made a couple of different non-isothermal measurements on sandstone, gypsum board and chipboard to determine whether moisture content is a driving force for surface diffusion or not. He compared isothermal and non-isothermal transport and found out that the moisture permeability decreases – as expected according to the hypothesis on the moisture content as a driving force for surface diffusion – when the moisture content gradient was opposite to water vapour pressure gradient. The same observation was achieved in the present study.

The experimental work reported in (Galbraith et al., 1998) included non-isothermal small-scale test on 2 different setups for $\varphi < 0.76$. The results from the first set-up on particle board and polystyrene insulation showed no consistent thermal diffusion. On the other hand, a second, improved set-up with a guard area for moisture transport showed very clear tendency for existence of thermal diffusion for plaster board and extruded polystyrene insulation. This temperature-induced transport made the total moisture transport higher, i.e. from warm to cold side. Also the influence of temperature on the moisture transport without a gradient was studied with modified cup measurements in (Galbraith et al., 1999). The effect of temperature turned out to be most clear for the most hygroscopic materials like MDF and plywood and especially at the higher relative humidity levels. This supports the theory that, at increasing levels of moisture content within the material, the effects of a temperature gradient will become more pronounced.

1.2 Dynamic boundary conditions

Dynamic simulation of the hygrothermal performance of building envelopes is widely used as a part of the building design process. The aim of these simulations is to predict how the designed construction will perform over the years exposed to naturally varying temperature and humidity loads. The materials are represented in the simulation models by their measured moisture properties, e.g. water vapour permeability, hydraulic conductivity and moisture retention. Common for all these properties is that they represent the material under steady state or equilibrium conditions.

Even though the used boundary conditions are dynamic, the common simulation models assume that there exists a local hygrothermal equilibrium within the material. This assumption makes it possible e.g. to convert local vapour pressure to moisture content of the material via sorption isotherm. It is widely accepted that this assumption is not necessarily quite correct, but for many materials the resulting error is assumed to be small. However, the assumption of immediate local moisture equilibrium ignores a possible time delay in the sorption processes - which can introduce significant errors in the modelling of the effects of rapid climate change.

Therefore, the central problem of these simulation models is the conflict between steady state material properties and the dynamic boundary conditions. For instance, the water vapour permeability of porous, absorbent materials is based on steady state measurements using the cup method. Such measurements do not involve water absorption by the material and are really just a measure of gas transmission through the physical pore structure. In practice, materials in the building envelope are exposed to naturally varying, non-isothermal conditions in both daily and annual time scale.

Chapter 2

Hypothesis

This experimental investigation will lead to some conclusions on the magnitude of moisture transport due to the temperature gradient on a range of porous light-weight building materials. An experimental method has been developed in an attempt to separate this 'other' moisture transport from the total measured moisture flux, and to quantify its significance relative to the water vapour pressure-driven transfer.

The aim of these actual measurements is also to identify the dynamic moisture response of a material exposed to a temperature gradient. The moisture capacity of the materials is defined as the slope of the sorption isotherm, which is based on the measurements of the equilibrium moisture content. The 'true' moisture capacity of the material is not necessary equal to this slope and is to be determined on the basis of the experimental results. It is understood that this way of presenting the problem is complex, as both the size of the moisture sorption capacity and the existence of the 'other' possible transport forms affect the resulting moisture transport and the distribution of moisture. Nevertheless, these measurements will help to understand the moisture conditions in building envelopes.

Chapter 3

Measurements

3.1 The equipment

A special climate chamber was constructed as described in (Padfield et al., 2001). In the following this chamber is called Megacup due to the similarity of the measurement principle with ordinary cups for water vapour permeability measurements, besides the size. The Megacup is a cylindrical well made of stainless steel (see Figure 3.1). The inner dimensions of the well are 793 mm (wide) and 500 mm (deep). The test specimen is suspended horizontally on the top of the chamber. On the bottom of the well there is a removable tray with a moisture control unit, climate sensors, fans and electrical connections. As a part of the moisture controller there is a water flux control system: The mass of a small open water container is weighted with given intervals. As the rest of the inner surfaces of the well are inert, the flux of moisture through the specimen can be determined by the change in the mass of water in the container. The construction details of the Megacup are given in (Padfield et al., 2002). The steel well is enclosed by an annular outer chamber. Air is circulated in this outer chamber to ensure an even temperature in the well to avoid condensation on the walls. The temperature of this air is controlled by an electric heater and a finned copper tube containing re-circulating cold water. The chamber humidity is controlled by another cold water system, which cools a heat pump. The steel well is well insulated around the periphery and under the bottom plate.

The climate in the chamber – temperature T and relative humidity RH – and the state of the different elements of the climate control system are measured continuously. The data is collected every minute by a data logger connected to a computer. An active program analyses the data and sends control signals to the data logger. The climate inside the Megacup can either be constant in respect to both T and RH or oscillating: 10-30°C and 40-95% RH. The overall set-up is illustrated in Figure 3.1(b). The lid of the chamber is made of rigid insulation, sealed vapour tight against the chamber. In the middle of the lid, there is a square hole of 0.5 x 0.5 meters where the test specimen is placed. The whole set-up is situated in a climate-controlled room, where temperature and relative humidity are held constant on the desired levels.

One of the objectives of this study was to investigate the local moisture distribution when a sample is exposed to a temperature gradient. Furthermore, the surface temperature and relative humidity conditions must be measured in order to reduce the uncertainties connected to the boundary layer effects. Therefore, small temperature and relative humidity sensors are inserted inside the material at 3 to 4 levels and on both surfaces (see Figure 3.2). Temperature is measured by K- and T-type thermocouples. Very small electronic relative

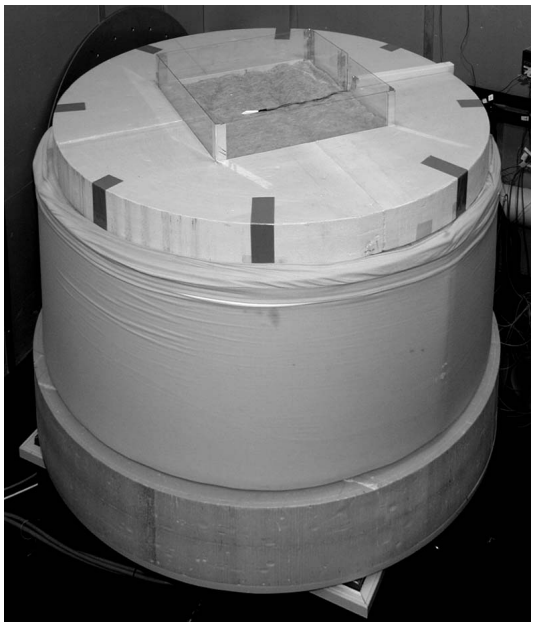

(a)

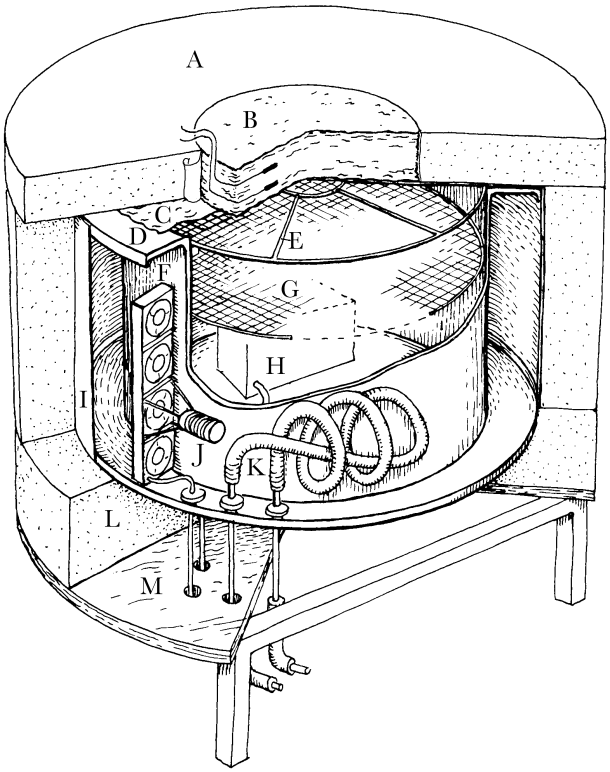

(b)

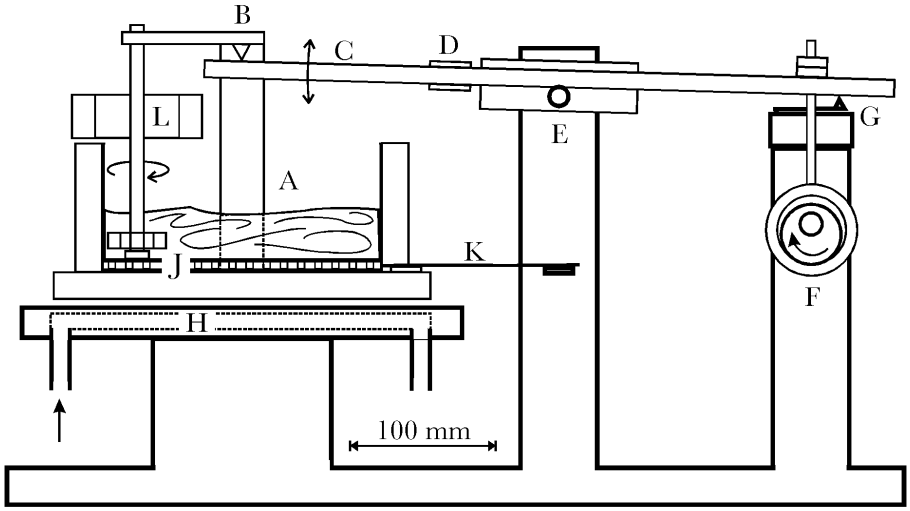

(c)

Figure 3.1: (a) The overall set-up with the Megacup. The specimen under test is the square piece inserted in the top. All that is visible of the Megacup is the exterior insulation and the sample. (b) The cross section of the experimental set-up and the construction principles: **A** thermal guard insulation **B** sample (normally square) **C** vapour barrier under the guard insulation **D** flange over annular space **E** open grid **F** fans **G** another grid (not used) **H** moisture control unit **I** aluminium wall **J** heating (electric resistance) **K** cooling (water circulating in coil) **L** bottom insulation **M** table. (c) The moisture control unit: **A** water container (copper) **B** suspension points **C** beam **D** strain gauge bridge **E** fulcrum **F** turning cam **G** microswitch to break the circuit **H** heat sink **J** thermoelectric heat pump **K** flat spring conductors **L** wind driven propeller. The illustrations are from (Padfield et al., 2002).

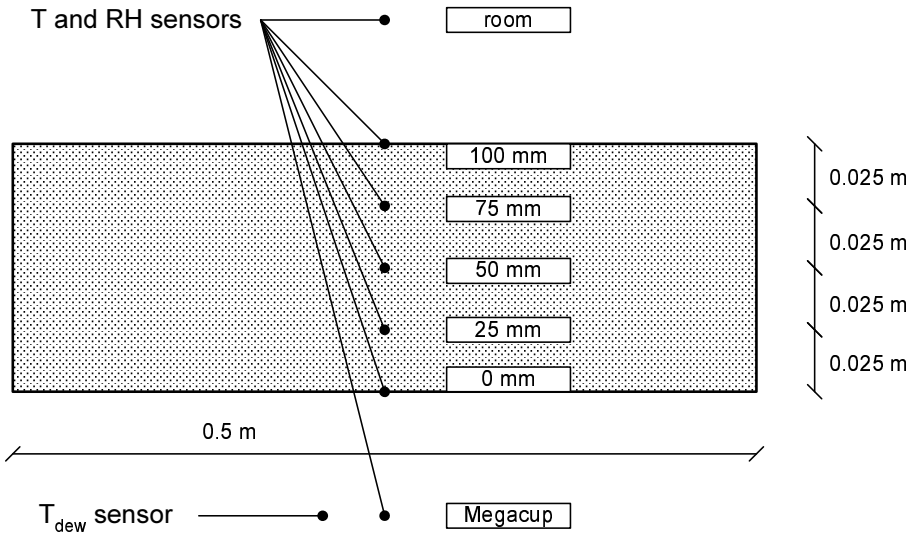

Figure 3.2: Location of the temperature and relative humidity sensors within the sample. Dimensions refer to samples with the thickness of 100 mm and sensors on 3 levels in the sample. Other thicknesses and sensor placements are used, too, but the indications of the sensors used for the results are always given in same way: The distance from Megacup surface (cold side) to room (warm side). Also the placement of the T_{dew}-sensor is given.

humidity sensors [1], which do not disturb the moisture flux, have been used. The relative humidity sensors measure voltage in a dielectric layer that is linearly dependent on the relative humidity of the ambient air. All the RH-sensors have been individually calibrated, both in respect to relative humidity and temperature. The unique feature with the used set-up is the possibility to measure the moisture flux into or out of the air of the chamber, g $[kg/(m^2 s)]$ by weighing the moisture controller within the Megacup, as described in (Padfield et al., 2002). A data logger averages and collects the 1-minute-measurements every 10 minutes. There is also a device, which makes it possible that water can be removed or applied to the moisture controller without opening the set-up, if that is needed.

The use of relative humidity sensors to measure the moisture conditions around and within the specimen is based on the assumption of local equilibrium, where the relative humidity in the pores of a porous material is in equilibrium with the water content of the material. This assumption is not necessarily correct under dynamic conditions, nor in steady state due to hysteresis. Therefore, the local moisture content cannot be fully estimated with the used relative humidity sensors.

3.2 Materials

Thermal insulating materials are supposed to be most suitable for this non-isothermal investigation, as they are capable to maintain a sufficient temperature gradient across the sample. With these materials also the effect of the thermal boundary resistance will be less dominating than for non-insulating materials. The materials selected for these tests are therefore: glass and rock wool insulation, cellular concrete and cellulose insulation.

Materials were chosen with the anticipation that some materials will show temperature-driven 'other' moisture transport, while others will not, and that they will respond very differently on the dynamic conditions. Moreover, the chosen materials are rather common

[1] HIH-3610 Series from Honeywell. http://content.honeywell.com/sensing/prodinfo/humiditymoisture. Dimensions: $3.8 \cdot 8.9 \cdot 0.6mm$

Table 3.1: Materials used in the non-isothermal Megacup tests. Material parameters for rock wool, cellulose, wool, flax and perlite are in general from (Hansen et al., 1999). Dry density for glass wool, cellular concrete and perlite are determined as a part of this work. The thermal conductivity for cellular concrete was determined as a part of student course work (Delfino and Giacchetti, 2001). Perlite was measured with 2 different sample thicknesses. Materials with * are granulates.

Material	**Dry density** ρ_0 $[kg/m^3]$	**Thermal conductivity** λ $[W/m \cdot K]$	**Thickness of the sample** d $[mm]$
glass wool	70	0.039	100
rock wool	30	0.039	100
cellular concrete	450	0.11	100
cellulose *	65	0.040	100
wool	25	0.039	100
flax	30	0.040	90
perlite *	100	0.050	100/140

in building envelopes. Some more exotic insulation materials are also included in the experiments: wool and flax insulation and expanded perlite. Table 3.1 introduces some of the material parameters together with the sample dimensions.

3.3 Measurement strategy

3.3.1 Steady state measurement strategy

The scope of this experimental work is to separate and quantify the transport forms involved in a non-isothermal moisture transport process. This is achieved by experiments where a temperature gradient together with different moisture gradients is created through a sample.

The material sample with a transmission area of 0.25 m^2 on the top of the Megacup – described in the previous Section – is exposed to a temperature gradient of 10 K and a given moisture gradient. The temperature on both sides of the sample has been fixed for all measurements: T_{room} = 22℃ and $T_{Megacup}$ = 12℃. The moisture flux in and out of the Megacup is registered continuously. In addition, the development in the local relative humidity and the local temperature is followed every minute by small sensors within the specimen and on both surfaces and in the ambient air, both in the Megacup and in the room (see Figure 3.2 for the principle placement of the sensors).

The moisture regulation strategy of the equipment depends on the desired moisture boundary conditions. One of the strategies to reveal any other transport than water vapour pressure driven one is to hold a constant weight of water in the moisture controller (see Figure 3.1(c)), which is equivalent to maintaining zero moisture flux through the specimen. The relative humidity inside the Megacup will reach the level where there is no flux - a value, which should correspond to the same vapour pressure as the one in the room - if there is no 'other' transport than vapour pressure-driven one. On the other hand, keeping a RH-gradient constant, but on different levels on each side, the boundary conditions are used to reveal any moisture transport due to the non-isothermal conditions. Altogether the used boundary conditions are:

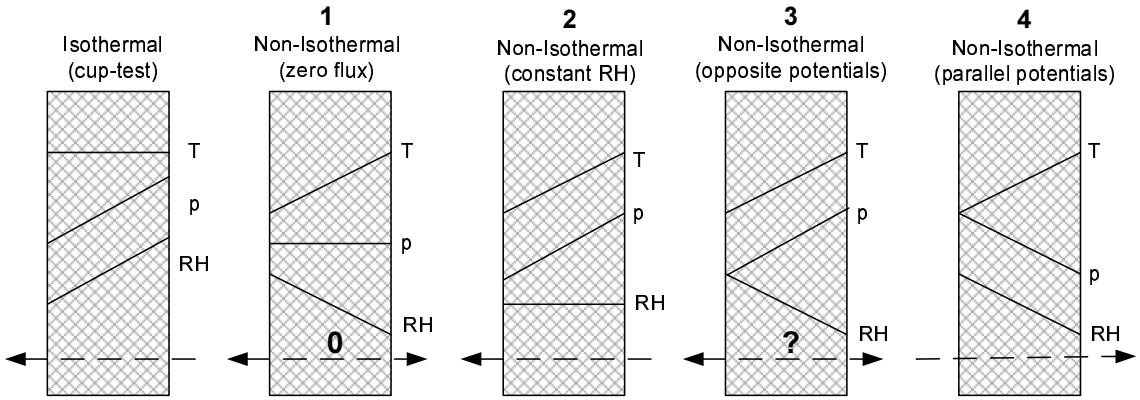

Figure 3.3: Steady state measurements. Illustration of the principle difference between isothermal and non-isothermal cup test on the moisture flow direction. Also the principal directions of gradients are shown for the four different measurement strategies. T is temperature, p water vapour pressure and RH relative humidity.

Table 3.2: Measurement strategy for non-isothermal, steady state measurements. The water vapour pressures are calculated from the temperatures and the relative humidities. $T_{room} = 22$℃ and $T_{chamber} = 12$℃. Water vapour pressure gradient Δp is set positive to the Megacup.

Measurement condition	**RH chamber** [%]	**RH room** [%]	**p Megacup** [Pa]	**p room** [Pa]	**Δp** [Pa]
1 Zero flux	?	45	?	1191	?
2 Constant RH	50	50	702	1323	621
3 Opposite potentials	75	50	1053	1323	270
4 Parallel potentials	90	40	1263	1058	-205

1. Zero flux: T- and RH-gradients are opposite, while p-gradient is supposed not to exist if there is only water vapour pressure-driven transport.

2. Constant relative humidity (RH): T- and p-gradients are in the same direction and there is no RH-gradient.

3. Opposite potentials: p- and RH-gradients are opposite, and T - gradient is in the same direction as p - gradient.

4. Parallel potentials: vapour pressure (p) and relative humidity (RH)gradients work parallel in the same direction, while T-gradient is opposite to the other gradients.

The impact of these gradients on the resulting moisture flux is presented principally in Figure 3.3, together with the illustration of the principle difference of isothermal and non-isothermal tests. Table 3.2 summaries the used boundary conditions and the measurement strategy.

3.3.2 Dynamic measurement strategy

The measurement strategy for the dynamic, non-isothermal tests is to expose a material sample to a sinusoidal change in relative humidity on the cold side with a period of 24 hours – see Figure 3.4 for the sinusoidal development in $RH_{Megacup}$. There are measurements on two different relative humidity levels: $65 < RH < 85\%$ and $75 < RH < 95\%$. The resulting

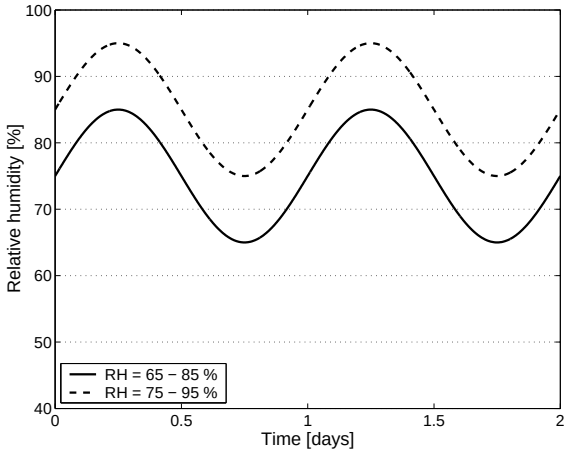

Figure 3.4: Dynamic measurements. The sinusoidal variation in the relative humidity of the Megacup air $RH_{Megacup}$. 2 different variations are used.

dynamic moisture sorption and transport process is then followed by built-in temperature and relative humidity sensors, together with the measurement of the net moisture flux through the sample.

One could have chosen to oscillate the temperature, as well or in stead of, but for sake of simplicity, the temperature was kept constant on both sides of the sample: $T_{room} = 22$℃ and $T_{Megacup} = 12$℃.

From the beginning, the plan was to test the materials on 2 different moisture levels – high dynamic relative humidity and low dynamic relative humidity – to see, if there exists any separate dynamic phenomenon for the high relative humidities. Unfortunately, it turned out during the tests that the temperature control of the equipment was not as stable as in the initial phase. This resulted in unwanted condensation on the Megacup inner walls, when $RH > 90\%$. Therefore the relative humidity conditions are not the same for all the materials.

3.4 Uncertainty

The accuracy of the setup is given in Table 3.3. Even though the accuracy of the set-up looks quite good, it must be kept in mind that the investigated 'other' transport effects are supposed to be rather small, and therefore it might turn out that even this accuracy is not enough. When evaluating the significance of the results, a possibility of uncertainties has to be recognised. In this Section, a range of possible errors and their impact on the results are discussed.

3.4.1 Moisture control

One of the main ideas in the design of the Megacup was the moisture control, where the water in the control unit always is the coldest place within the whole set-up. Using this method, no uncontrolled condensation occurs and the measured flux is an accurate representation of the actual flux produced by the driving potentials. The regulation strategy of the Megacup is ruled by a computer program, which at the moment is based on a rather simple algorithm using a first order PID-control. For some climate conditions the relative humidity in the Megacup is oscillating ($\Delta RH = \pm 1.5\%$) while it for some other conditions is quite stable

Table 3.3: Accuracy of the Megacup equipment and the used sensors. For humidity control the range in accuracy is due to the different accuracy on different RH-levels, the accuracy being best for low RH.

Component	**Accuracy**
Humidity control	$\pm$ 0.25 – 1.5% RH
Temperature control	$\pm$ 0.2K
Moisture flux control	0.001 g
Temperature sensors	$\pm$ 0.2 K
Relative humidity sensors	$\pm$ 1.5% RH (calibrated sensors)

($\Delta RH = \pm 0.25\%$). A 'window' of as stable environmental conditions as possible is used to obtain an accurately measurable flux. Unfortunately, the moisture controller has a limited capacity: It was difficult to measure very permeable materials, therefore, thicker samples and smaller transmission areas should be used. The humidity in the room is controlled by a PID controlled system connected to a humidifier and a dehumidifier. This system has performed satisfactorily enough.

Furthermore, to double-check the results in the end of the measurements, the vapour pressure on the both sides of the specimen (room and Megacup) was also measured by a dew point measuring device [2]: Air from the room or from the Megacup was circulated through the dew point meter. In this way one of the typical errors could be reduced: The use of different transducers for different measurements. This check was done when a steady state had been reached. The results from these measurements showed (Figure 3.5) that when T_{dew} was uniform both in Megacup and in the room, the used RH-sensors gave a standard deviation in vapour pressure of around $\sigma = 35Pa$. Resulting standard deviation for the relative humidity sensors becomes $1.5 - 2.5\%RH$.

However, this 'final calibration' shows that the used relative humidity sensors underestimate heavily the RH on the cold side. This is also illustrated in Figure 3.6, where all the sensors are placed in a same climate and should therefore show the same relative humidity. While the small sensors agree quite well on the resulting RH, the 'true' level – measured with 2 different dew point sensors – is much higher for the low temperatures. Therefore, the RH-measurements are assumed to fulfill the expected standard deviation *relatively* to each others, while the *absolute* value on the cold side of the sample is very uncertain.

The accuracy of the strain gages is in principle up to 0.001 g. However, the measured weight of water is oscillating surprisingly lot. Whether this is a result of weighing accuracy – more realistically at 0.1 g – or the oscillating humidity or temperature in the Megacup, is not clear. In order to give a more clear picture of the behavior, the measurements are presented using running averages.

3.4.2 Temperature control

The temperature in the Megacup is controlled as described in Section 3.1. The main disadvantage of this system is the asymmetry of the regulation: The cooling is water based and has got a large thermal inertia while heating is based on electrical resistance and has a very low inertia. Regulating this kind of system is very challenging and a certain temperature oscillation has been accepted ($\Delta T = \pm 0.2K$). The resulting RH-oscillation becomes

[2] Michell Dew point sensor

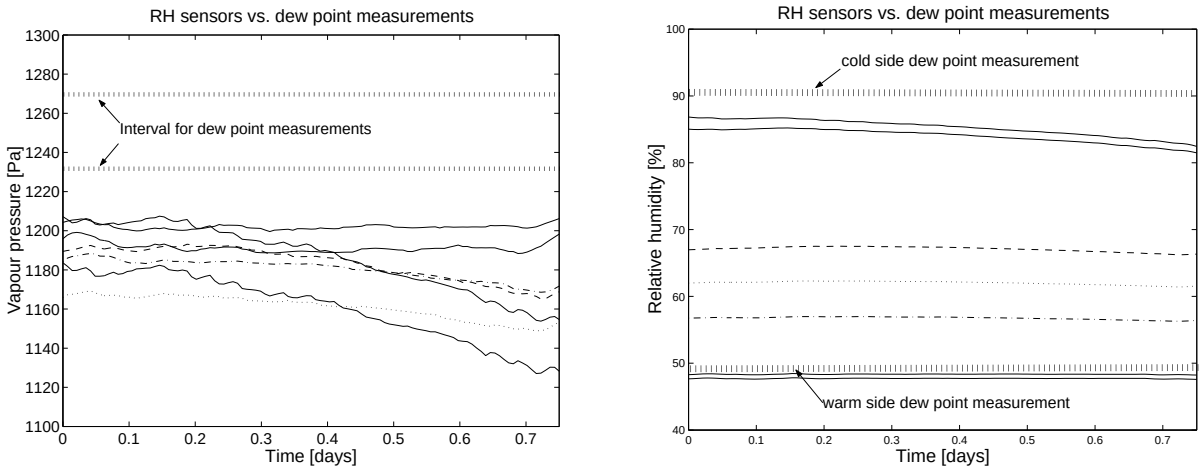

(a) (b)

Figure 3.5: A measurement sequence for glass wool, where the T_{dew} both in room and in Megacup has been measured for the shown time period. The measured T_{dew} was practically uniform for all the cases. (a) The deviation in the vapour pressure based on measurements with the small relative humidity sensors is 50–100 Pa and lies clearly at a lower level than p according to dew point measurements. (b) Resulting RH shows that the RH measured with the small sensors on the warm side is very close to the dew point measurements, while the RH on the cold side is underestimated with the small sensors.

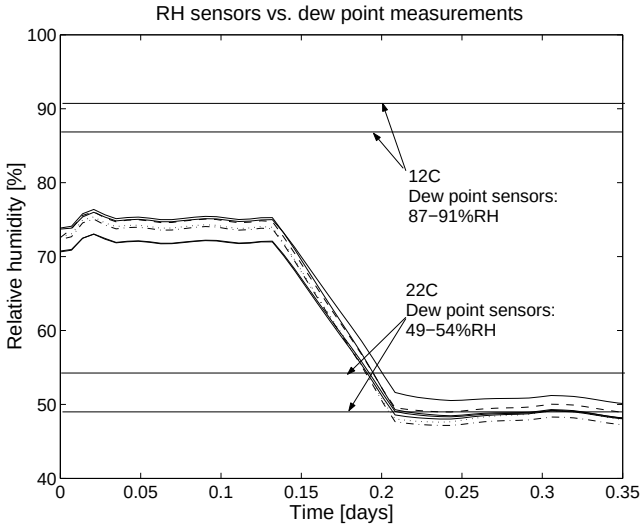

Figure 3.6: A measurement sequence, where all the small RH-sensors together with 2 different dew point sensors have been first inside the Megacup (12℃) and then in the room (22℃). The deviation is very large on the cold side and the small RH-sensors underestimate the relative humidity in great extend.

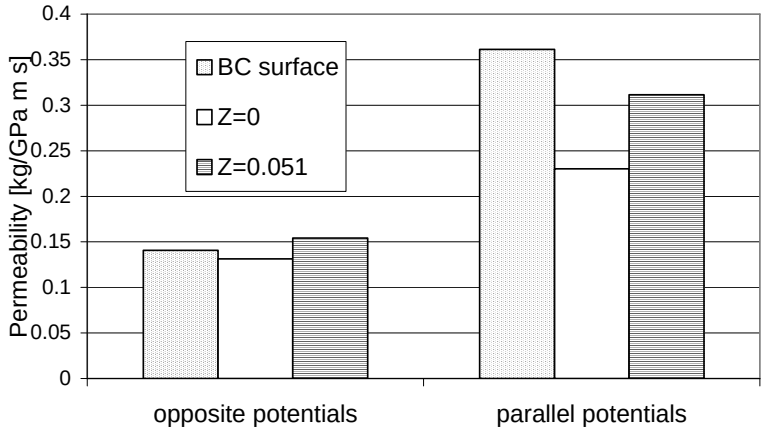

Figure 3.7: The effect of the determination of boundary conditions on the calculated permeability for flax under 2 different moisture resistances Z = 0 $(GPa \cdot m^2 \cdot s)/kg$ and Z = 0.05 $(GPa \cdot m^2 \cdot s)/kg$ and Δp based on the state of the ambient air. These cases are compared with the actual measurements, where the measured surface conditions are used directly to determine the permeability (BC surface).

$\Delta RH = \pm 1\% RH$. Temperature in the room is very stable and maintained by a water-based heating and cooling aggregate..

3.4.3 Measurement of boundary conditions

To reduce uncertainties of the measured results, it is important to know the surface temperature and moisture conditions as exactly as possible. An attempt to measure these surface conditions has been the aim for all the measurements with the Megacup. The unknown convective surface moisture resistance will hereby be eliminated as a source of error. To illustrate the significance of this, an example is given in Figure 3.7, where apparent permeability calculated based on measured surface conditions (BC surface) is compared with the apparent permeability calculated with 2 arbitrary chosen different convective moisture transfer resistances Z = 0 $(GPa \cdot m^2 \cdot s)/kg$ and Z = 0.05 $(GPa \cdot m^2 \cdot s)/kg$ and Δp $[Pa]$ is based on the state of the ambient air. Equation 3.1 gives the permeability when there is a moisture transfer resistance Z on both surfaces:

$$\delta_p = \frac{d}{\frac{\Delta p}{g} - (Z_{p,in} + Z_{p,out})} \tag{3.1}$$

where δ_p $[kg/(Pa \cdot m \cdot s)]$ is the water vapour permeability, d $[m]$ thickness of the sample and g $[kg/(m^2 s)]$ the moisture flux. The resulting permeability is especially for the case with parallel potentials quite sensitive to how the boundary conditions are defined and measured.

Chapter 4

Results

4.1 Steady state measurements

4.1.1 Apparent permeability

The apparent water vapour permeability δ_p $[kg/(Pa \cdot m \cdot s)]$ is calculated with Equation 4.1 under the assumption that water vapour pressure is the only driving force for moisture transport:

$$\delta_p = g \cdot \frac{d}{\Delta p} \tag{4.1}$$

where Δp $[Pa]$ is the water vapour pressure gradient calculated from the measured relative humidity and temperature on both surfaces of the sample, g $[kg/(m^2 \cdot s)]$ the total moisture flux and d $[m]$ the thickness of the sample. Table 4.2 shows the calculated apparent permeability under 3 different boundary conditions: constant RH, opposite and parallel potentials. These values can be compared with isothermal permeabilities in Table 4.1. According to the isothermal measurements reported in (Hansen et al., 1999), the isothermal permeability of rock wool, cellulose, wool, flax and perlite is not a function of relative humidity and therefore only a value for wet-cup measurements ($50\% < RH < 93\%$) is given here. Isothermal permeabilities for glass wool and cellular concrete have been measured as a part of the present work as dry-cup and wet-cup, and no significant dependence on relative humidity was found here, either. It is stressed that the determined apparent permeabilities for constant relative humidity $\delta_{p,RH}$, opposite $\delta_{p,opp}$ and parallel potentials $\delta_{p,par}$ only serve to give the first idea of the magnitudes, and are not seen as 'material parameters'.

These apparent permeabilities are plotted together with the isothermal permeabilities as a function of RH-distribution, see Figure 4.1. These measurements show no correlation between the RH and the permeability, but they illustrate the effect of parallel potentials on the apparent permeability: $\delta_{p,par}$ is two to eight times greater than the one for opposite potentials $\delta_{p,opp}$. The values for opposite potentials and constant RH are relatively close to the isothermal permeability. The standard deviation[1] for calculated permeabilities is up to $\pm 4.4 \cdot 10^{-11}$, which makes $\delta_{p,opp}$ and $\delta_{p,RH}$ to be treated as uniform with isothermal permeability, while $\delta_{p,par}$ is significantly different.

[1] Standard deviation for δ_p σ_{δ_p} is determined with an analytical expression, where both σ_g and $\sigma_{\Delta p}$ and the partial derivates of δ_p are included.

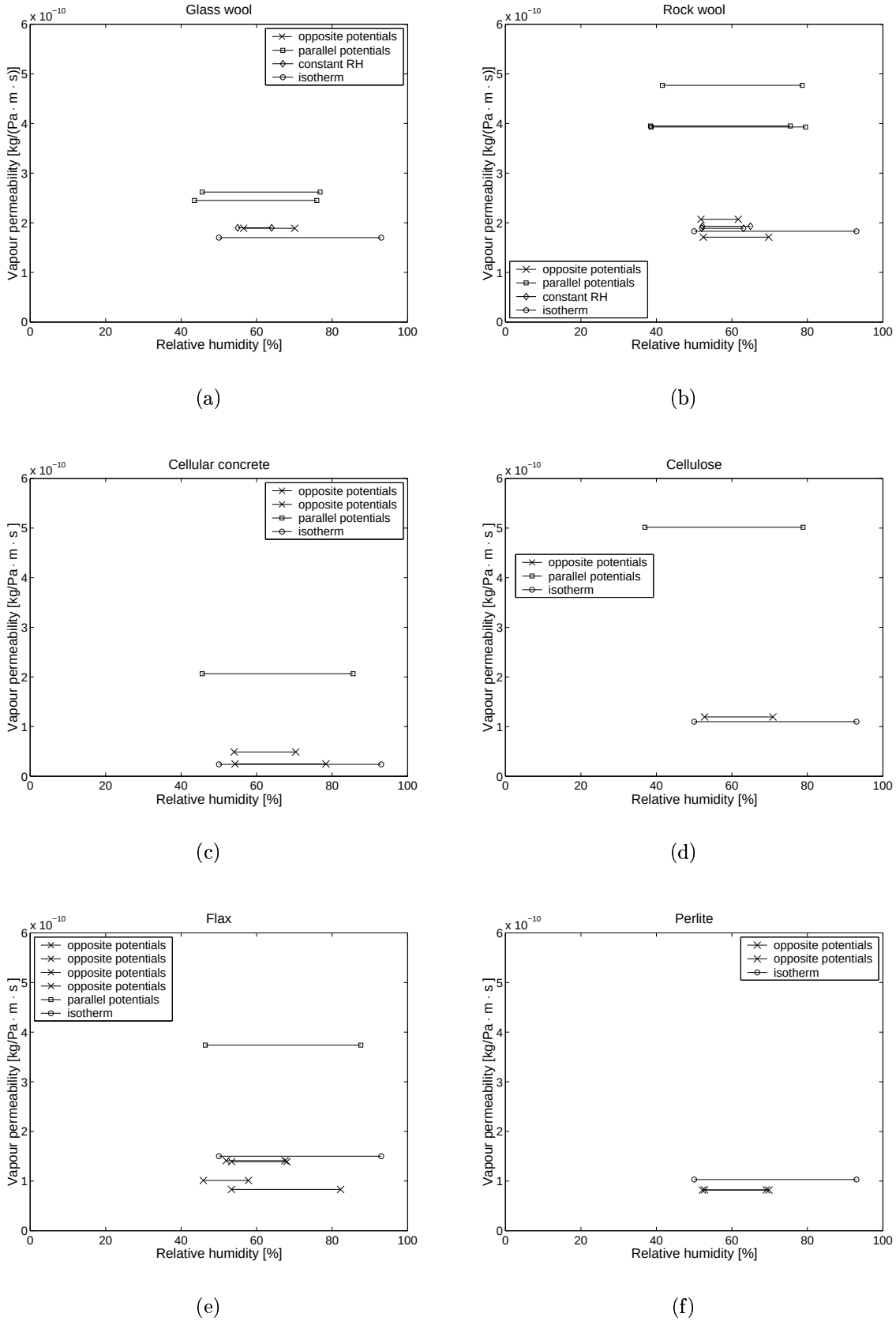

Figure 4.1: Measured isothermal and apparent permeabilities for (a) glass wool insulation, (b) rock wool insulation, (c) cellular concrete, (d) cellulose insulation, (e) flax insulation and (f) expanded perlite. Note: The absence of parallel potentials for perlite. Boundary conditions: constant RH (condition **2**, only for glass wool and rock wool), opposite potentials (condition **3**) and parallel potentials (condition **4**).

Table 4.1: Isothermal water vapour permeability for the investigated materials. Isothermal permeabilities originate from (Hansen et al., 1999), except for glass wool and cellular concrete that have been determined as a part of this work with the same experimental set-up and conditions as in (Hansen et al., 1999). There were used 6 samples for each condition, except 3 and 4 samples for glass wool and cellular concrete, respectively. The isothermal permeabilities are values from wet-cup measurements: $50\% < RH < 93\%$.

Material	**Isothermal permeability** δ_p $[kg/(Pa \cdot m \cdot s)]$
glass wool	$(0.170 \pm 0.01) \cdot 10^{-9}$
rock wool	$(0.183 \pm 0.03) \cdot 10^{-9}$
cellular concrete	$(0.024 \pm 0.0004) \cdot 10^{-9}$
cellulose	$(0.110 \pm 0.002) \cdot 10^{-9}$
wool	$(0.190 \pm 0.052) \cdot 10^{-9}$
flax	$(0.150 \pm 0.059) \cdot 10^{-9}$
perlite	$(0.103 \pm 0.015) \cdot 10^{-9}$

Table 4.2: Apparent water vapour permeability calculated from the non-isothermal Megacup test results, calculated under assumption of that the water vapour pressure gradient is the only driving force.

Material	**Apparent non-isothermal permeability**		
	Constant RH (condition **2**) $\delta_{p,RH}$ $[kg/(Pa \cdot m \cdot s)]$	Opposite potentials (condition **3**) $\delta_{p,opp}$ $[kg/(Pa \cdot m \cdot s)]$	Parallel potentials (condition **4**) $\delta_{p,par}$ $[kg/(Pa \cdot m \cdot s)]$
glass wool	$0.19 \cdot 10^{-9}$	$0.19 \cdot 10^{-9}$	$0.25 - 0.26 \cdot 10^{-9}$
rock wool	$0.19 \cdot 10^{-9}$	$0.17–0.21 \cdot 10^{-9}$	$0.39–0.48 \cdot 10^{-9}$
cellular concrete	-	$0.023–0.045 \cdot 10^{-9}$	$0.19 \cdot 10^{-9}$
cellulose	$0.13 \cdot 10^{-9}$	$0.12 \cdot 10^{-9}$	$0.50–1.0 \cdot 10^{-9}$
wool	-	$0.14 \cdot 10^{-9}$	$0.35 \cdot 10^{-9}$
flax	-	$0.083–0.14 \cdot 10^{-9}$	$0.37 \cdot 10^{-9}$
perlite	$0.093 \cdot 10^{-9}$	$0.068–0.072 \cdot 10^{-9}$	-

This gives strong indications that there must exist other transport than the water vapour pressure-driven one.

Strictly, the apparent permeability calculated according to Equation 4.1 from the measured Δp describes only water vapour transport, but it is assumed here that it might also include liquid transport. However, the separation of liquid and vapour contributions is not possible here on the basis of the measurements and therefore the 'other' transport is given as 'bulk' transport of vapour and liquid.

The isothermal permeability at $\delta_p = 0.183 \cdot 10^{-9}$ for rock wool and the apparent permeability for constant RH (condition **2**) at $\delta_{p,RH} = 0.189\text{-}193 \cdot 10^{-9}$ are identical within the accuracy of the measurements. Under isothermal conditions p- and RH-gradients are parallel and if there is any liquid transport, this is parallel with the pure water vapour diffusion. Under constant RH, the T-gradient is parallel to p-gradient. On the basis of these conditions it is not possible to conclude, which of the other gradients is giving the 'other' transport.

For opposite potentials (condition **3**) there is a T-gradient parallel with p-gradient, while the RH-gradient is opposite. This condition gives the slightly lowest apparent permeability at $\delta_{p,opp} = 0.171\text{-}208 \cdot 10^{-9}$ for rock wool, indicating that there must be some transport driven

Table 4.3: The magnitude of moisture transport against vapour pressure gradient for the investigated materials. The 'other' transport is determined as the intersection with the y-axis of the trend line in Figure 4.2.

Material	**'Other' transport** $[kg/(m^2 s)]$
glass wool	$1.6 \cdot 10^{-7}$
rock wool	$2.4 \cdot 10^{-7}$
cellular concrete	$1.5 \cdot 10^{-7}$
cellulose	$3.7 \cdot 10^{-7}$
flax	$0.45 \cdot 10^{-7}$
perlite	$1.2 \cdot 10^{-7}$

by the RH-gradient.

Finally, when compared with the other conditions, the apparent permeability for condition **4** becomes high, $\delta_{p,par}$=0.39-0.48$\cdot 10^{-9}$ for rock wool, because now the RH-gradient does not just work against the water vapour pressure-driven transport but supports it. The direction of the temperature gradient-driven transport is not known on the basis of this analysis, but it can be noticed here that the direction of total flux in this case is from cold to warm.

4.1.2 'Other' transport

In addition, to illustrate that there exists a moisture flux induced by other driving forces than water vapour pressure gradient, the measured moisture flux g is plotted as a function of Δp, together with the 95% confidence intervals. Figure 4.2 shows this. The trend is clear: The trend line corresponding to the different magnitudes of water vapour pressure gradient and moisture flux intersect the zero vapour pressure gradient not at the zero moisture flux, but at a negative flux. This negative moisture flux at Δp=0 can be seen as an indication for that there is a transport against the p-gradient. The investigated materials seem to belong to 2 groups: cellular concrete, perlite, rock wool and cellulose insulation have rather significantly 'another' transport against the water vapour pressure gradient, while the significance is minor for flax and non-existing for glass wool.

The deviation from zero flux for zero water vapour pressure in Figure 4.2 can be evaluated directly as 'another' moisture transport. The magnitude of this transport against vapour pressure gradient is given in Table 4.3.

The presented results so far have given a strong indication for that also gradients of both T and RH play a role for the total non-isothermal moisture transport. There can be developed a hypothesis on how the 'other' transport could be allocated to the identified potentials: 3 single contributions to the total transport are given as

$$g = g_{diffusion} + g_{liquid} + g_{thermal} \tag{4.2}$$

where $g_{diffusion}$ stands for pure water vapour diffusion, while g_{liquid} represents any liquid transport and $g_{thermal}$ any temperature gradient induced transport. This hypothesis is presented and discussed in (Peuhkuri, 2003).

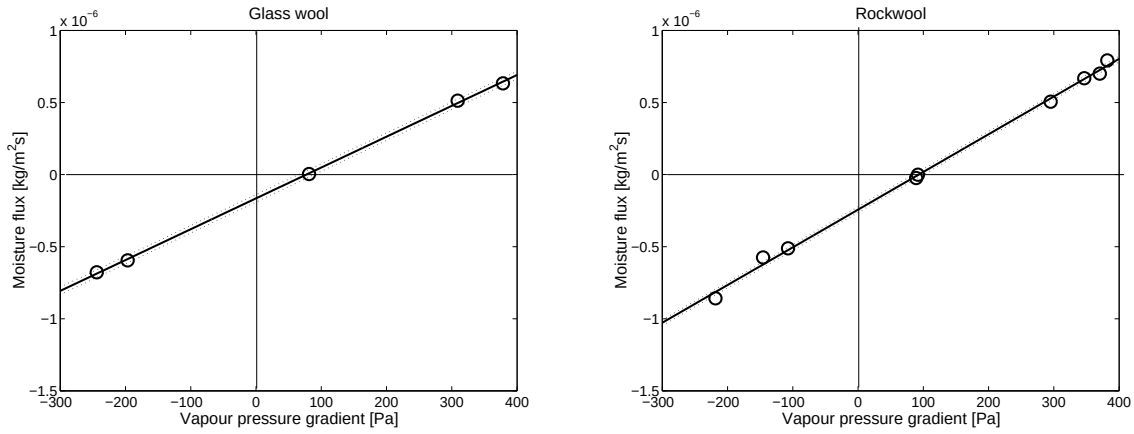

(a)

(b)

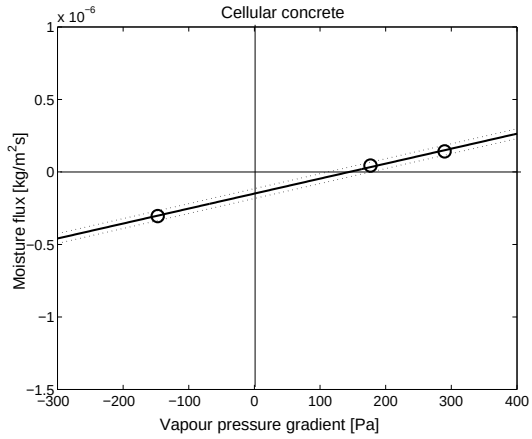

(c)

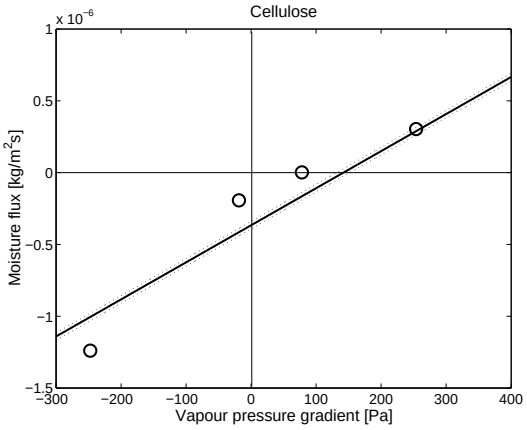

(d)

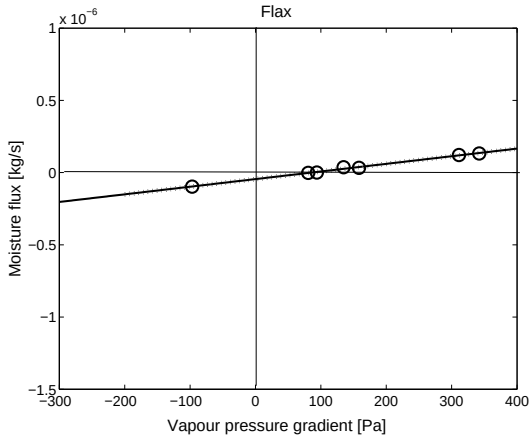

(e)

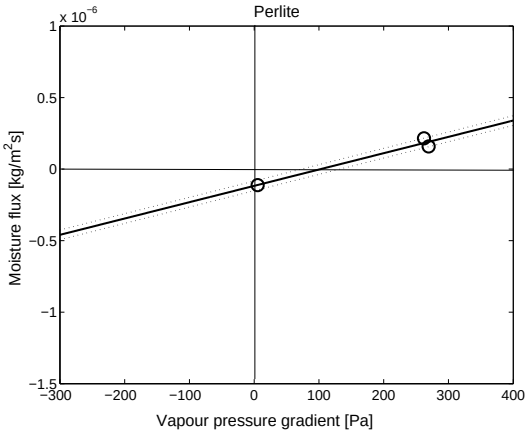

(f)

Figure 4.2: Moisture flux (g) as a function of water vapour difference (Δp) for (a) glass wool insulation, (b) rock wool insulation, (c) cellular concrete, (d) cellulose insulation, (e) flax insulation and (f) expanded perlite. All measurement conditions are used for the measured values (circles) and the linear trend lines (—). 95 % confidence intervals are given with (...). Confidence intervals were determined from the calculated standard deviation for flux measurements at $\sigma_g = 3 \cdot 10^{-8} kg/(m^2 s)$ and the number of observations.

Table 4.4: The measured relative humidity RH in Megacup is compared with the theoretical relative humidity in Megacup, which would be the case if the only driving potential is the gradient of water vapour pressure Δp or water vapour concentration ρ_v, when there is no net moisture flux (condition **1**). The RH-value measured with a dew point sensor inside the chamber, is closer to the 'true' RH than the small sensors and gives an indication for the great uncertainty of the measured values.

	Megacup relative humidity[%]			
	Measured		**Theoretical**	
Material	small RH-sensors	T_{dew}-sensor	Δp=0	$\Delta \rho_v$=0
glass wool	81	89	88	86
rock wool	81	89	88	86
cellular concrete	87	90	94	91
cellulose	80	87	88	85
flax	93	95	97	94
perlite	76	79	84	81

4.1.3 Resulting relative humidity and vapour pressure profiles

The distribution of RH and p in the material for different boundary conditions is given in Figure 4.3 for rock wool insulation. The profiles can be compared with the principle profiles introduced in Figure 3.3. Temperature profiles are not shown, but they are practically identical for all cases.

Relative humidity and vapour pressure profiles in Figure 4.3 show that RH and p are almost linear. This is the case for all the materials. However, the small tendency to non-linearity of p can be explained by the uncertainties in the measured RH, which gives a standard deviation for p at $34Pa$. It is seen that deviations from linearity for p are within this value and therefore the water vapour pressure profiles can be assumed linear. The non-linear nature of saturation vapour pressure p_{sat} due to the strong temperature dependence plays a role for the RH-profiles, and makes RH decrease relatively quickly for increasing temperature. Therefore, this non-linearity of RH-profiles is expected and not an indication of any other transport.

4.1.4 Resulting $RH_{Megacup}$

Finally, for the condition, where no net moisture flux was measured (condition **1**), resulting RH in Megacup is given in Table 4.4.

The investigation of the resulting relative humidity in the Megacup, when net moisture flux was zero, is presented in Table 4.4. If the RH measured with the dew point sensor – which is assumed to give more reliable values than the small RH-sensors – is compared with the theoretical RH for Δp=0, hardly any difference is found. The only materials showing any significant difference at all are cellular concrete and perlite. For ρ_v=0, even this significance disappears.

Therefore, the existence of a transport against Δp-gradient, which could make the resulting RH on the cold side lower than expected, making a building envelope more resistent to damage due to excessive moisture loads, cannot be confirmed with these observations. Also previous laboratory tests reported in (Vinha et al., 2002) showed that hygroscopic insulation materials like cellulose and flax performed not significantly better in avoiding high moisture levels than mineral wool in a building envelope structure without a vapour barrier.

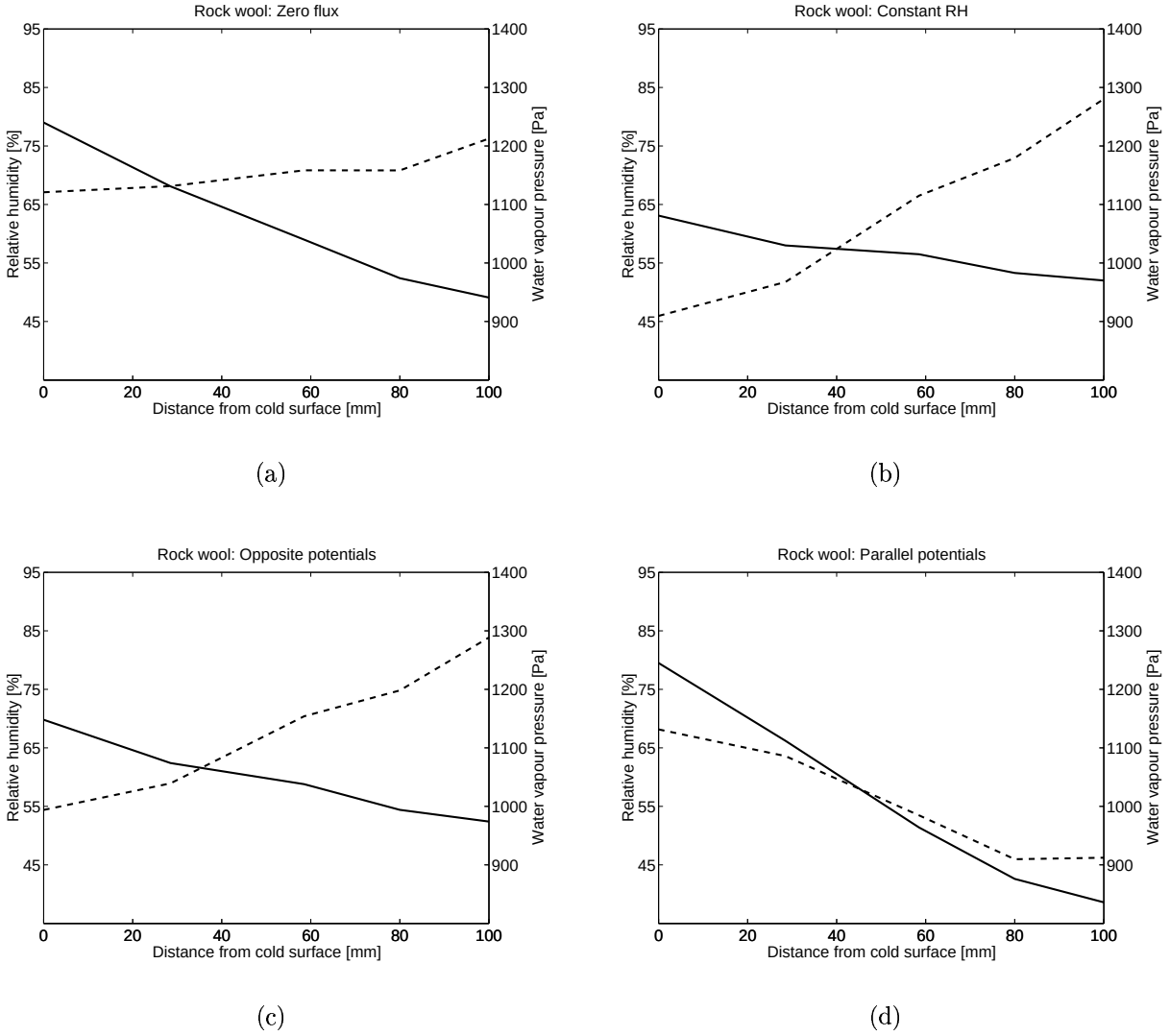

Figure 4.3: Measured relative humidity (solid line) and vapour pressure (dotted line) profiles for rock wool insulation for boundary conditions, where the profiles are a result of the given boundary conditions: (a) **1** zero flux, (b) **2** constant RH, (c) **3** opposite potentials and (d) **4** parallel potentials. Note that the resulting RH is not constant in case (b). This is due to a limited capacity of the moisture controller for reducing the $RH_{Megacup}$.

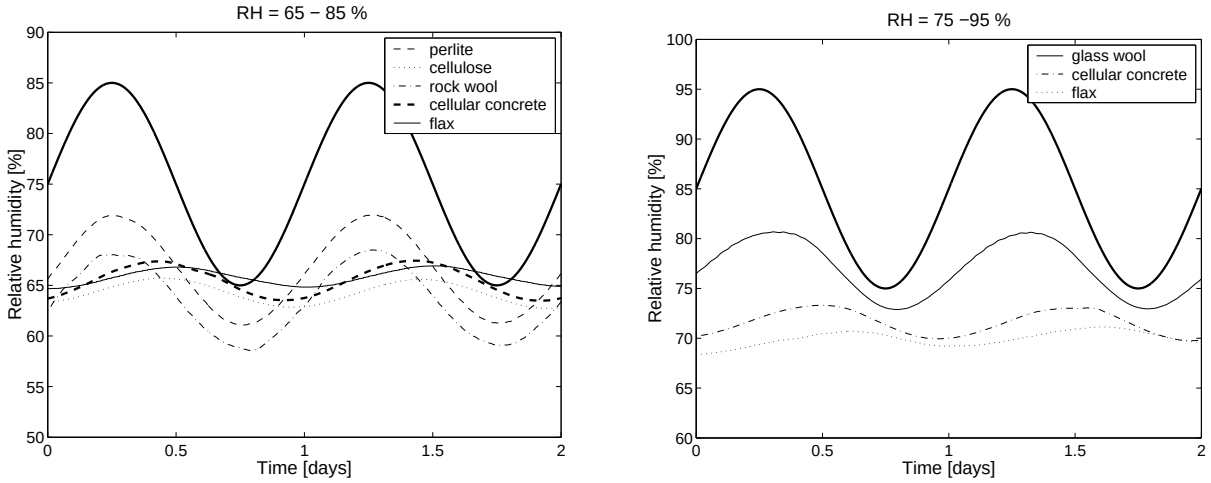

(a) (b)

Figure 4.4: The measured relative humidity approximately $28mm$ from the cold surface for sinusoidal variation (a) $RH = 65 - 85\%$ and (b) $RH = 75 - 95\%$ in Megacup (thick solid line). Exact distances are: Cellulose $26mm$, cellular concrete $27.5mm$, perlite $28mm$, rock wool $28.5mm$, flax $29mm$ and glass wool $30mm$.

4.2 Dynamic measurements

Figures 4.5 and 4.6 show the development in relative humidity in the different layers of the samples during a 48-hour-period. Values in Figure 4.5 are a result of a sinusoidal oscillation in $RH_{Megacup}$ between 65 and 85 $\%RH$ while they in Figure 4.6 come from oscillations between 75 and 95 $\%RH$. Note that the sensor locations are not identical from material to material.

A comparison of the dynamic response on the cold side of the material between the different materials is illustrated in Figure 4.4. The curves are almost comparable the materials in-between: The shown development in relative humidity corresponds to location $26 - -30mm$ from the cold surface. There are 2 main observations:

1. The response is remarkably more buffered for cellulose, cellular concrete and flax insulation than for perlite, glass wool and rock wool.

2. The phase delay is greatest for cellulose, descending hereafter for flax, cellular concrete, glass wool, rock wool and finally perlite, which does not have any phase delay at all

The phase delay for cellulose, cellular concrete and flax insulation increases with distance from the cold surface and the oscillating climate.

4.2.1 Resulting moisture flux

The resulting total net moisture flux is calculated from the weight change of the moisture controller and is illustrated as an comparison of different materials in Figure 4.7. The amount of moisture involved in the interaction between the material and the air in Megacup as a response to the oscillations is in this way illustrated. It is quite obvious that for rock wool, glass wool and perlite samples, there is much less moisture involved than for the other

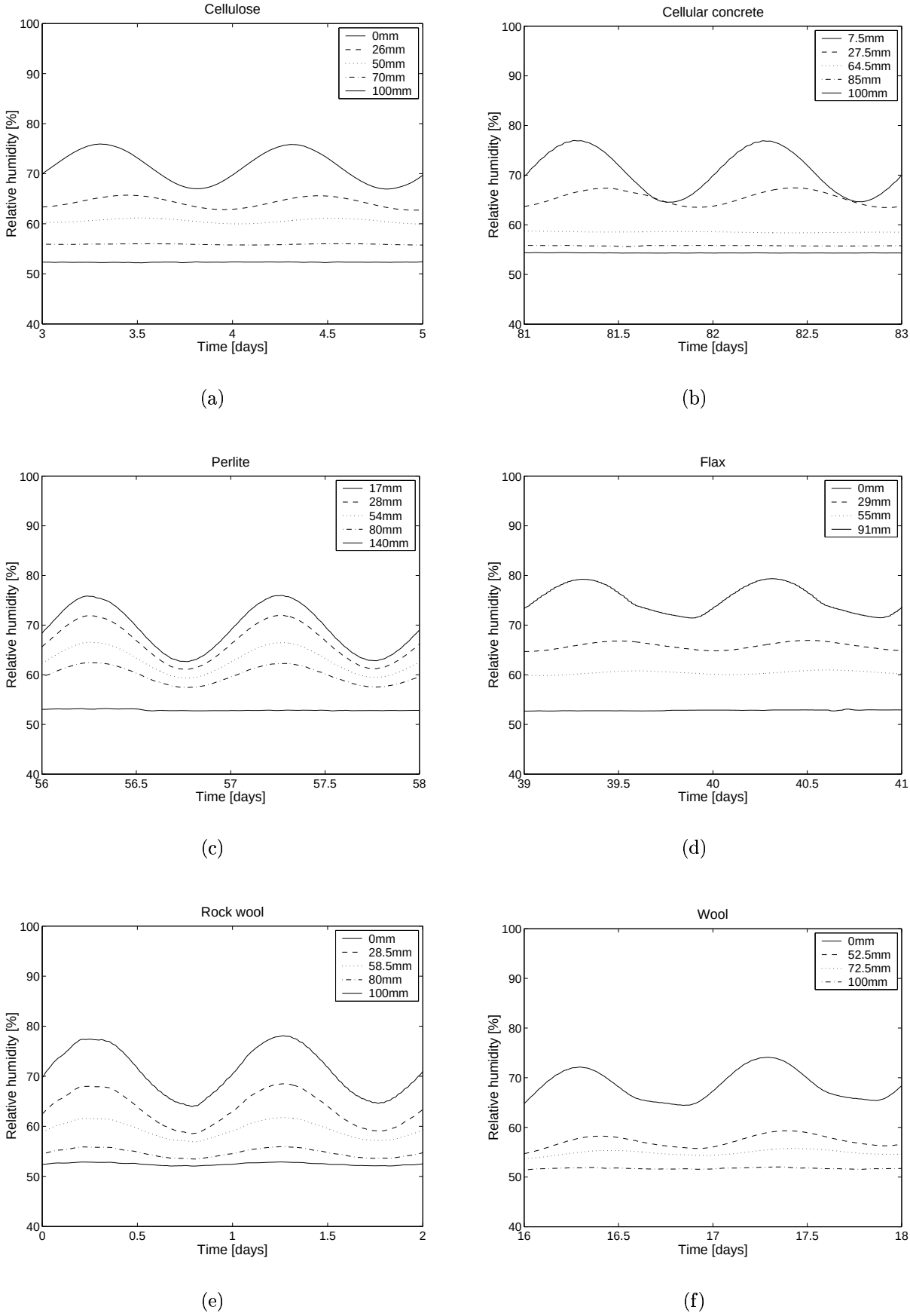

Figure 4.5: The measured distribution of relative humidity for sinusoidal variation $RH = 65 - 85\%$ for (a) cellulose (b) cellular concrete (c) perlite, (d) flax, (e) rock wool and (f) wool insulation. Note that the sinusoidal variation for flax is not symmetrical. This is due to problems with the capacity of the moisture controller. Legends stand for the sensor distance from the cold surface of the sample.

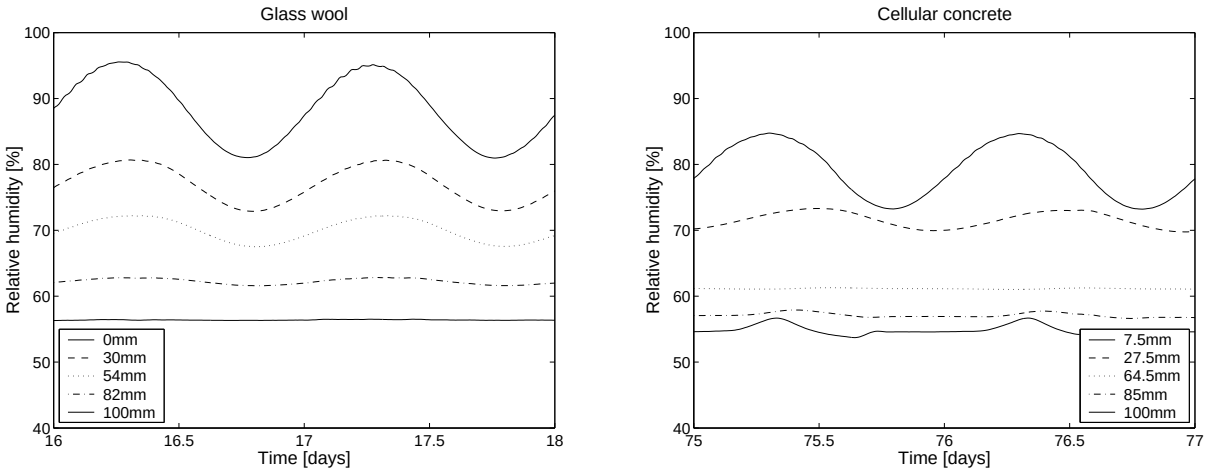

(a) (b)

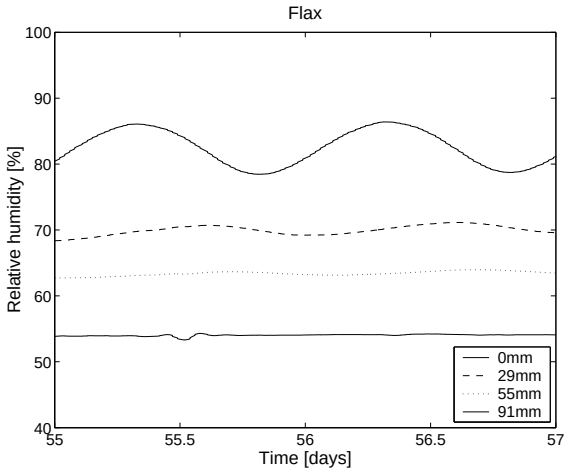

(c)

Figure 4.6: The measured distribution of relative humidity for sinusoidal variation $RH = 75 - 95\%$ for (a) glass wool (b) cellular concrete (c) flax.

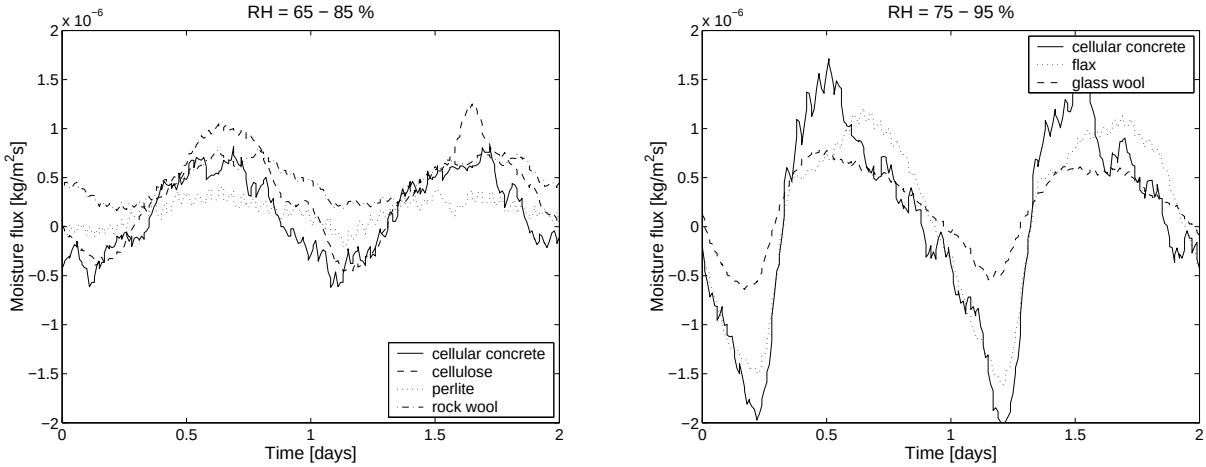

(a) (b)

Figure 4.7: Comparison of the measured moisture flux $[kg/m^2s]$ for the different materials. (a) Sinusoidal variation $RH = 65 - 85\%$ (b) Sinusoidal variation $RH = 75 - 95\%$.

Table 4.5: The measured and theoretical 'penetration depth' d_p for non-isothermal, sinusoidal oscillations in the Megacup for $RH = 65 - 85\%$. The measured d_p is a result of a fitting of the measured p-distribution (calculated from the measured RH and T) with the theoretical solution for a slab exposed to a sinusoidal variation in water vapour pressure, see details in (Peuhkuri, 2003). The penetration depth was defined as a depth from the cold side, where the oscillations in RH were 36.7 % of the oscillations on the material surface, here the cold side. The theoretical d_p was determined from Equation 4.3.

Material	**Penetration depth** $[mm]$	
	measured	**theoretical**
glass wool	55	52
rock wool	>100	104
cellular concrete	32	9
cellulose	37	18
wool	$\sim$ 100	42
flax	35	27
perlite	85	90

materials. Furthermore, cellulose and cellular concrete make more water to move than than flax. The curve for glass wool is not totally comparable with the other materials as RH_{room} for glass wool tests was lower, which also makes the flux smaller.

4.2.2 Penetration depth

Another way of representing the difference between the materials is to determine their penetration depth d_p $[m]$, i.e. the depth at which oscillations in RH are less than a certain fraction, here chosen to be 36.7% of the oscillations in ambient air. It can be calculated analytically as:

$$d_p = \sqrt{\frac{D_w t_p}{\pi}} = \sqrt{\frac{\delta_p \cdot p_{sat} \cdot t_p}{\rho_0 \cdot \xi \cdot \pi}} \tag{4.3}$$

where D_w $[m^2/s]$ is the moisture diffusivity, t_p $[s]$ a period of the sinusoidal oscillations, p_{sat} $[Pa]$ saturation water vapour pressure, ρ_0 $[kg/m^3]$ dry density and ξ [-] the moisture capacity of the material. For these actual measurements, d_p has also been measured directly, determined from the measured RH-oscillations inside the sample by fitting with a theoretical solution for a slab. This analysis is given in more detail in (Peuhkuri, 2003). These depths – both the theoretical and the measured ones for RH=65 – 85% – are given in Table 4.5.

The main observation was that the 'measured' penetration depth d_p, defined as a measure for the sinusoidal oscillations being less than 36.7% of the oscillations on the cold surface of the material at this location, was greatest for materials like perlite and glass wool, and smallest for materials like cellulose and flax insulation. This means that the material that was on the 'warm side' of this depth could not 'feel' more than about one third of the changes in the relative humidity in the Megacup. Subsequently, within this 'inactive' part of the materials there existed almost steady state conditions in terms of moisture ab- and desorption. The level of relative humidity changes, low or high, did not seem to influence the penetration depth. The measured RH-range involved inside the material during a period of 24 hours is illustrated in Figure 4.8 for cellulose and rock wool, together with the 'measured' and theoretical penetration depth.

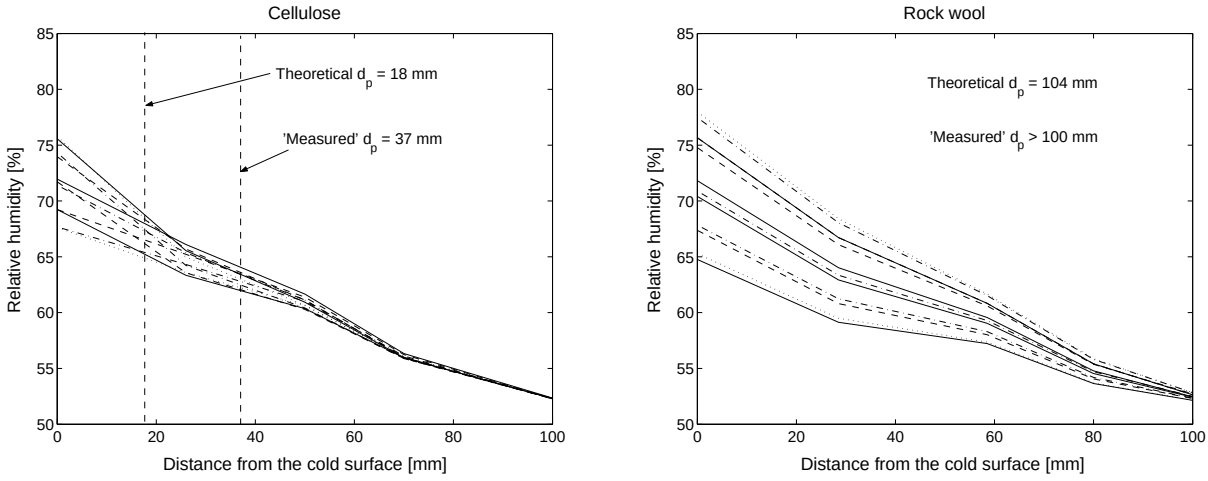

(a) (b)

Figure 4.8: The measured relative humidity as a function of distance from the cold surface for sinusoidal variation in the Megacup $65 - 85\%RH$ for (a) cellulose and (b) rock wool. The different curves are values for different times during a 24-hour-period. Also the 'measured' and theoretical penetration depth is given.

The theoretical d_p is significantly smaller than the 'measured' one for the materials like cellular concrete, cellulose and wool insulation. For the materials like glass wool, rock wool, flax and perlite there is almost no difference.

4.2.3 Buffer capacity

A material's ability to absorb or release moisture is sometimes called the moisture buffer capacity of the materials, and is a function of permeability and the absorptive power of the material. This ability is interesting for example when designing (partly) passive indoor climate regulation strategies or when studying the robustness of a construction against interstitial condensation. In the following, there are presented two different ways of characterising the moisture buffer capacity of the materials.

Moisture accumulation capacity

The buffer capacity of the materials can be determined as the moisture accumulation capacity b_m $[kg/(m^2 Pa\sqrt{s})]$ theoretically given by Equation 4.4.

$$b_m = \sqrt{\frac{\delta_p \cdot \rho_0 \cdot \xi}{p_{sat}}} \tag{4.4}$$

By rearranging, this equation can be expressed as Equation 4.5, which includes the 'measured' d_p. In this way the moisture accumulation capacity b_m can also be given as a 'measured' value. Both the theoretical and the measured values for b_m are given in Table 4.6 and in Figure 4.9.

$$b_m = \frac{d_p \cdot \rho_0 \cdot \xi}{p_{sat}} \sqrt{\frac{\pi}{t_p}} \tag{4.5}$$

Table 4.6: Theoretical and 'measured' values for moisture accumulation capacity b_m. Theoretical values are calculated from Equation 4.4 and the 'measured' ones from Equation 4.5. The slope of the sorption isotherm is determined from the isothermal sorption experiments presented in (Peuhkuri, 2003). The 'measured' penetration depth is given in Table 4.5. Values are valid for $RH = 65-85\%$.

Material	**Slope of sorption isotherm** [-]	**Moisture accumulation capacity** $[10^{-7} kg/(m^2 Pa\sqrt{s})]$	
	average	**measured**	**theoretical**
glass wool	0.057	6	5
rock wool	0.036	3	3
cellular concrete	0.045	17	5
cellulose	0.32	20	10
wool	0.28	18	8
flax	0.46	12	9
perlite	0.008	2	2

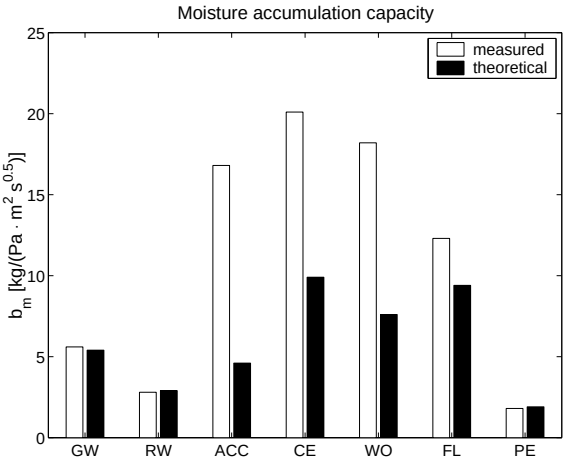

Figure 4.9: Theoretical and 'measured' values for moisture accumulation capacity b_m for all the measured materials.

Available water

The moisture buffer capacity of the materials is also calculated from Equation 4.6 for both theoretically and as a 'measured' value. d_p for the 'measured' case is the measured value and the theoretical d_p for the theoretical case given in Table 4.5. These theoretical and 'measured' values for Δm_w $[[kg/(m^2 \cdot \Delta\varphi \cdot t_p)]]$ are compared in Table 4.7. The moisture capacity ξ in both cases is determined from the equilibrium moisture content.

$$\Delta m_w = \rho_0 \cdot \xi \cdot \Delta\varphi \cdot d_p \tag{4.6}$$

But what does this buffer capacity of the material mean? It means that materials like cellulose and flax insulation and cellular concrete are able to moderate the oscillations in relative humidity on the cold side. Oscillations in relative humidity in a building construction as a such are usually not dangerous, but a great oscillation means often also high peaks in the relative humidity. Figure 4.4 illustrates this: moderated RH results in a lower peak values of the relative humidity. For instance, the resulting peak relative humidity $28mm$ from the cold side is around $5\%RH$ lower for cellular concrete or flax – and 7-8$\%RH$ lower for cellulose – than for expanded perlite insulation or glass wool.

A comparison of resulting relative humidity on the cold surface, at $0mm$, would be most

Table 4.7: The available water calculated from Equation 4.6. The slope of the sorption isotherm is determined from the isothermal sorption experiments presented in (Peuhkuri, 2003). Penetration depth is measured from the non-isothermal tests in the Megacup given in Table 4.5. These dynamic, non-isothermal values are compared with the theoretical values based on the theoretical d_p given by Equation 4.3. $\Delta RH = 10\%$ has been chosen as an arbitrary value for comparison. Values are valid for $RH = 65 - 85\%$.

Material	**Available water** $[g/(m^2 \cdot 10\%RH \cdot 24h)]$	
	measured	**theoretical**
glass wool	22	21
rock wool	11	11
cellular concrete	65	18
cellulose	78	39
wool	71	29
flax	48	36
perlite	7	7

interesting, but this was not possible for all the materials due to the different locations of the sensors. The moisture response on this cold surface is here illustrated with rock wool and cellulose insulation in Figure 4.10. Consequently, materials with a good buffer capacity, are slightly more resistant to damage due to high moisture loads than constructions with glass wool and perlite, but this is not significant, especially on the cold, and most critical surface. Here, the difference in peak values in-between these very different materials is only $2\%RH$, which can be regarded as a non-significant difference due to the uncertainties of the measurements.

Therefore, the difference between hygroscopic and non-hygroscopic materials is not significant, especially on the cold and most critical surface. In addition, it seems that there has been a drift in the measured RH towards a lower RH-level during the measurement series. Therefore, the comparison of the different materials might be misleading.

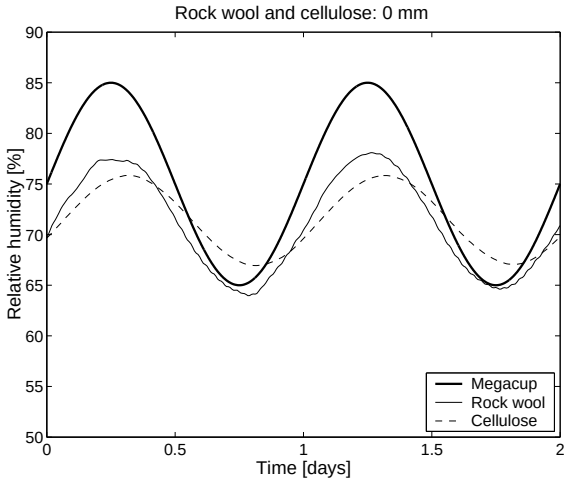

Figure 4.10: The response of cold – and the most critical – surface of rock wool and cellulose insulation on a sinusoidal variation in the relative humidity of the Megacup air at $65 < RH < 85\%$.

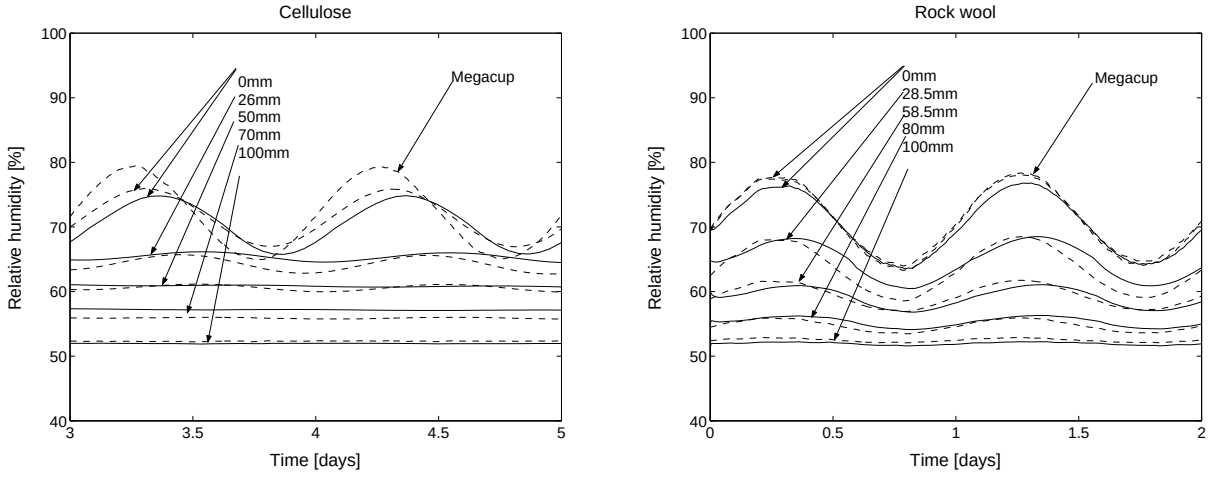

(a) (b)

Figure 4.11: Comparison of measured (dotted lines) and simulated (solid lines) distribution of relative humidity. The measured relative humidity has been used as boundary condition in the Megacup. (a) Cellulose $RH = 65 - 85\%$ and (b) rock wool $RH = 65 - 85\%$.

4.2.4 Simulations

The measurements are compared with the results from numerical simulations. The simulation model is based on the same partial differential equations and material parameters as in the MATCH model (Rode, 1991). The documentation of the conventional simulation model is found in detail in (Peuhkuri, 2002). The model used to the present results do not include hysteresis, but uses average of ab- and desorption isotherms. Significance of hysteresis is studied for cellulose.

The simulation results with the measured relative humidity as the boundary condition show – Figure 4.11 – that there is a fairly good agreement between the measurements and simulations for cellulose, perlite and flax insulation. A slight phase delay is seen for the simulation results for all the materials. This indicates a smaller moisture capacity in the dynamic case than the one determined from the slope of the sorption isotherm or the existence of remarkable hysteresis effect. The results could also indicate that the permeability of the materials is greater than the value determined with isothermal cup-measurements, which is the permeability used in the model.

A possible explanation for this deviation could also be the use of relative humidity sensors and the assumption of the local equilibrium between the absorbed moisture and the humid air in the simulation model. The true moisture content of the material is not necessarily corresponding to the measured RH, while they in the simulation model do correspond. Therefore the measure RH changes slightly more rapidly than the corresponding moisture content of the material. This observation can also be seen as an indication for that the true moisture capacity is smaller than the mathematical one, the reason being either non-Fickian behaviour and/or hysteresis effect.

Significance of hysteresis

There have been used average of ab- and desorption isotherms in the simulations so far. Some of the observed deviations between measurements and simulations might be explained with the hysteresis effect. The significance of the hysteresis will be illustrated here for a

single material: cellulose insulation (see Figure 4.12) for 2 different multiplications of the slope of the scanning curve: scanning curve slope = slope · 0.4 and slope · 0.6. The hysteresis model is described in (Peuhkuri, 2002) together with the entire model. Here is also found discussion about the choice of the slope of the scanning curve, which by (Chomcharn and Skaar, 1983) is recommended to be multiplied with 0.4.

Figure 4.12(a) illustrates how a hysteresis model with a slope multiplied with 0.4 almost eliminates the phase delay compared to the model without hysteresis. This is due the reduced moisture capacity as a result of this reduced slope. However, the reduced moisture capacity results also in an increased amplitude of RH. Figure 4.12(b) shows how the increased moisture capacity (slope multiplied with 0.6) results in deviation in phase delay between measurements and simulations that, however, is not as large as for the model without hysteresis.

Therefore, including hysteresis in the model, reduces the deviations between modelling and measurements in some extend but do not explain the deviations totally.

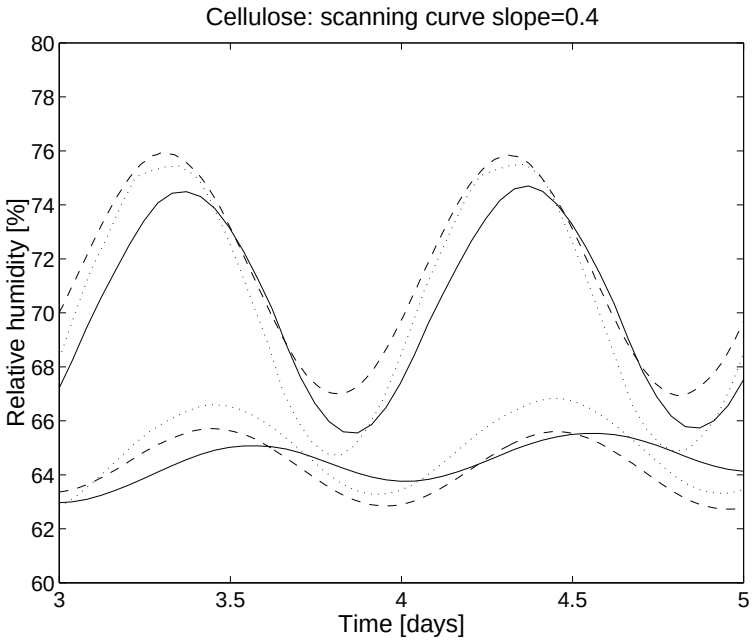

(a)

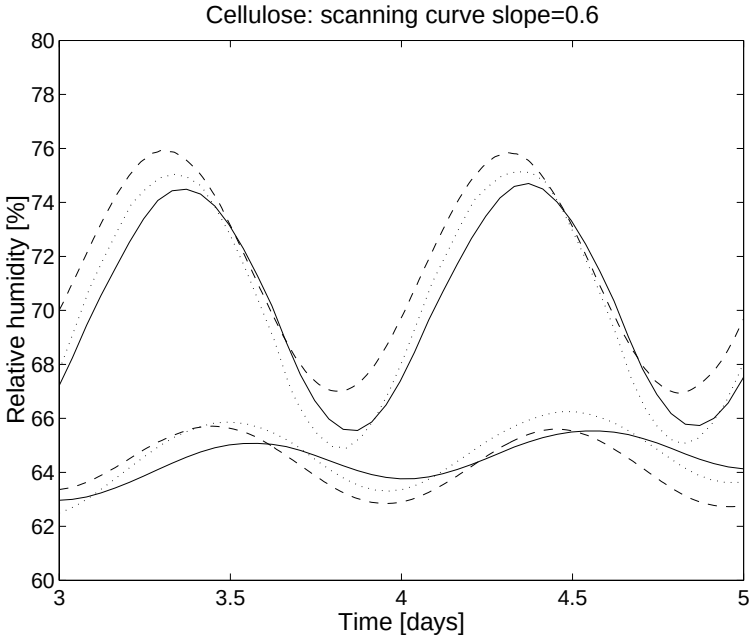

(b)

Figure 4.12: Comparison of measurements (- - -), simulations without (—) and with hysteresis (....) for cellulose. RH-oscillations are given for locations: $0mm$ and $26mm$. Conventional model is used. Simulation without hysteresis uses an average of ab- and desorption isotherms. Hysteresis is investigated for 2 different slopes of the scanning curve: (a) scanning curve slope = slope $\cdot$ 0.4 and (b) scanning curve slope = slope $\cdot$ 0.6.

Chapter 5

Conclusion

The results until now showed that there exists some kind of 'other' transport against Δp in all the analysed materials. However, the results could not support the common assumption for hygroscopic insulating materials, like cellulose insulation, that they are able to protect themselves from too excessive moisture levels on the cold side of a building envelope. Rather surprisingly, all the materials, as well the almost non-hygroscopic materials (e.g. rock wool) as the very hygroscopic materials (e.g. cellulose insulation) showed the same characteristics. However, the returned data suffered from unstable measurements and, subsequently, the amount of data cannot be seen as sufficient for drawing any definite conclusions. Nevertheless, the trend of results seems rather convincing.

Materials like cellulose and flax insulation and cellular concrete were able to moderate the oscillations in RH more than glass wool, rock wool and perlite. The moderated RH also resulted in a slightly lower general level and the peak values of the relative humidity, making constructions with cellular concrete and flax and especially cellulose marginally more resistent to damage due to high moisture loads than constructions with rock wool, glass wool and perlite. For instance, the resulting relative humidity $28mm$ from the cold side is up to $5\%RH$ lower for a construction with cellular concrete or flax – and up to 7-8$\%RH$ lower for a construction with cellulose – than a construction with expanded perlite insulation or glass wool. This difference between the materials, however, is not assumed to be significantly unambiguous, especially when the discussed accuracy of the used small RH-sensors is kept in mind.

Moisture buffer capacity of the materials was also assessed. It turned out that the 'measured' buffer capacity was higher than the theoretical buffer capacity for the materials with good buffer capacity: flax, wool and cellulose insulation and cellular concrete. There was no difference for materials with poor buffer capacity: glass wool, rock wool and perlite.

The comparison of the measured and simulated results showed that there for the most of materials exist a fairly good agreement with the used conventional, Fickian model. A minor phase delay on simulated results indicates that the true moisture capacity of the materials is lower than the mathematical one – the slope of the sorption isotherm. Implementing hysteresis in the model will reduce the moisture capacity and increase the agreement between measurements and simulations.

References

Chomcharn, A. and Skaar, C. (1983). Dynamic sorption and hygroexpansion of wood wafers exposed to sinusoidally varying humidity, *Wood Science and Technology* **17**: 259–277.

Delfino, S. and Giacchetti, G. (2001). Assignment in master course, '11546 Experimental Mechanics' at Department of Civil Engineering at Technical University of Denmark.

Galbraith, G. H., Guo, J. S. and McLean, R. C. (2000). The effect of temperature on the moisture permeability of building materials, *Building Research and Information* **28**(4): 245–259.

Galbraith, G. H., Guo, J. S., McLean, R. C., Lee, C. K. and Kelly, D. J. (1999). The temperature dependence of moisture permability, *CIB W40 Conference*, Prague.

Galbraith, G. H., McLean, R. C., Gillespie, I., Guo, J. S. and Kelly, D. (1998). Nonisothermal moisture diffusion in porous building materials, *Building Research and Information* **26**(6): 330–339.

Hansen, E. J., Hansen, K. K. and Padfield, T. (1999). Measured moisture properties for alternative insulation products, *5th Symbosium on Building Physics in the Nordic Countries*, Göteborg.

Krus, M. (1995). *Feuchtetransport- und Speicherkoefficienten poröser mineralischer Baustoffe. Theoretische Grundlagen und neue Meßtechniken*, PhD thesis, Fakultät Bauingeneur- und Vermessungswesen der Universität Stuttgart.

Kumaran, M. K. (1988). Comparison of simultaneous heat and moisture transport through glass-fibre and spray-cellulose insulations, *Journal of Thermal Insulation* **12**: 6–16.

Padfield, T. (1999). *The role of absorbent building materials in moderating changes of relative humidity*, Ph.d thesis (Report no.54), Department of Structural Engineering and Materials, Technical University of Denmark.

Padfield, T., Peuhkuri, R., Rode, C. and Hansen, K. K. (2002). Non-isothermal water vapour transmission through porous insulation. Part 1: Equipment, *6th Symbosium on Building Physics in the Nordic Countries*, Trondheim.

Padfield, T., Rode, C., Nicolajsen, A. and Hansen, K. K. (2001). Udstyr til undersøgelse af fugtfordeling i absorberende isoleringsmaterialer, *Sagsrapport SR-0028*, Technical University of Denmark, Department of Buildings and Energy. http://www.ens.dk/graphics/isolering/99-13.pdf.

Peuhkuri, R. (2000). *Isoleringsmaterialers fugttekniske egenskaber i klimaskærm (Moisture performance of insulation materials in building envelopes)*, Master's Thesis, Technical University of Denmark, Department of Buildings and Energy.

Peuhkuri, R. (2002). SIMULINK model of coupled heat and moisture transport in material layers, *Report SR-02-02, Department of Civil Engineering, Technical University of Denmark.*

Peuhkuri, R. (2003). *Moisture dynamics in building envelopes*, PhD thesis, Department of Civil Engineering, Technical University of Denmark (To be published).

Rode, C. (1991). Description of the model MATCH. theoretical background, equations (T1-DK-91/01), *IEA Annex 24 Final report, Volume 1: Task 1: Modelling.*

Vinha, J., Käkelä, P. and Lindberg, R. (2002). Moisture tranport in timber-framed external wall structures in nordic climate. Laboratory tests, *6th Symbosium on Building Physics in the Nordic Countries*, Trondheim.

Appendiks B

Moisture distribution in absorbent insulation - Description of the dataset and its use

The following list shows the available dataset.

Wool.xls	1.604.096 bytes	02-05-03 17.26
Glass wool.xls	1.628.160 bytes	30-04-03 16.23
Cellular concrete.xls	16.296.960 bytes	23-04-03 13.26
Perlite.xls	4.668.928 bytes	23-04-03 10.28
Cellulose.xls	4.859.392 bytes	23-04-03 10.26
Flax.xls	8.167.936 bytes	23-04-03 10.25
Rock wool.xls	1.632.256 bytes	23-04-03 10.24

Below is shown an example on how the measured data are presented. The first column gives the time in days beginning from the time when the moisture flux starts. The last seven columns are in this example the temperature (**T**) in °C in different places, which also is indicated by the name of the worksheet. Other measured data are relative humidity (**RH**) in %RH and the moisture flux (**flux**) in kg/(m^2·s). There is also a worksheet that gives the vapour pressure (**p**) in Pa, but it is calculated by use of the temperature and the relative humidity.

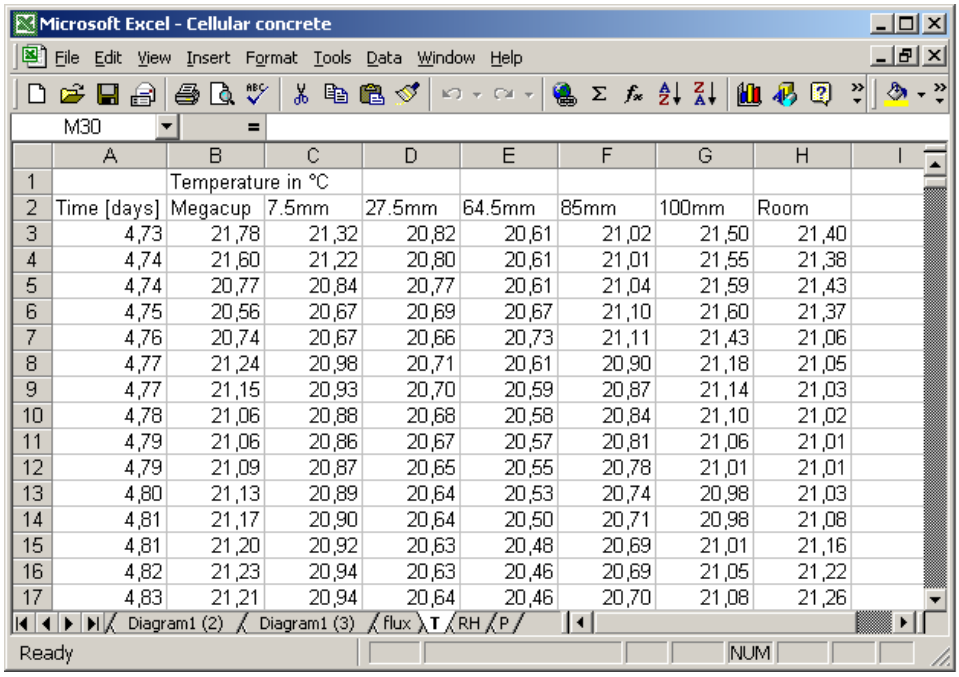

	A	B	C	D	E	F	G	H	I
1		Temperature in °C							
2	Time [days]	Megacup	7.5mm	27.5mm	64.5mm	85mm	100mm	Room	
3	4,73	21,78	21,32	20,82	20,61	21,02	21,50	21,40	
4	4,74	21,60	21,22	20,80	20,61	21,01	21,55	21,38	
5	4,74	20,77	20,84	20,77	20,61	21,04	21,59	21,43	
6	4,75	20,56	20,67	20,69	20,67	21,10	21,60	21,37	
7	4,76	20,74	20,67	20,66	20,73	21,11	21,43	21,06	
8	4,77	21,24	20,98	20,71	20,61	20,90	21,18	21,05	
9	4,77	21,15	20,93	20,70	20,59	20,87	21,14	21,03	
10	4,78	21,06	20,88	20,68	20,58	20,84	21,10	21,02	
11	4,79	21,06	20,86	20,67	20,57	20,81	21,06	21,01	
12	4,79	21,09	20,87	20,65	20,55	20,78	21,01	21,01	
13	4,80	21,13	20,89	20,64	20,53	20,74	20,98	21,03	
14	4,81	21,17	20,90	20,64	20,50	20,71	20,98	21,08	
15	4,81	21,20	20,92	20,63	20,48	20,69	21,01	21,16	
16	4,82	21,23	20,94	20,63	20,46	20,69	21,05	21,22	
17	4,83	21,21	20,94	20,64	20,46	20,70	21,08	21,26	

The second column with the indication “Megacup” gives the measurement within the megacup. The third column has the indication 7.5 mm, which is the distance from the inner surface of the megacup to the place of the given sensor, the same is the case for the columns 4, 5, 6 and 7. The last column named “Room” gives the measured data in the surrounding climate chamber.

The worksheet named **flux** only gives the measured flux from the megacup.

Besides the data worksheets there is one or more worksheets named **diagram**. The diagram is presented like the following.

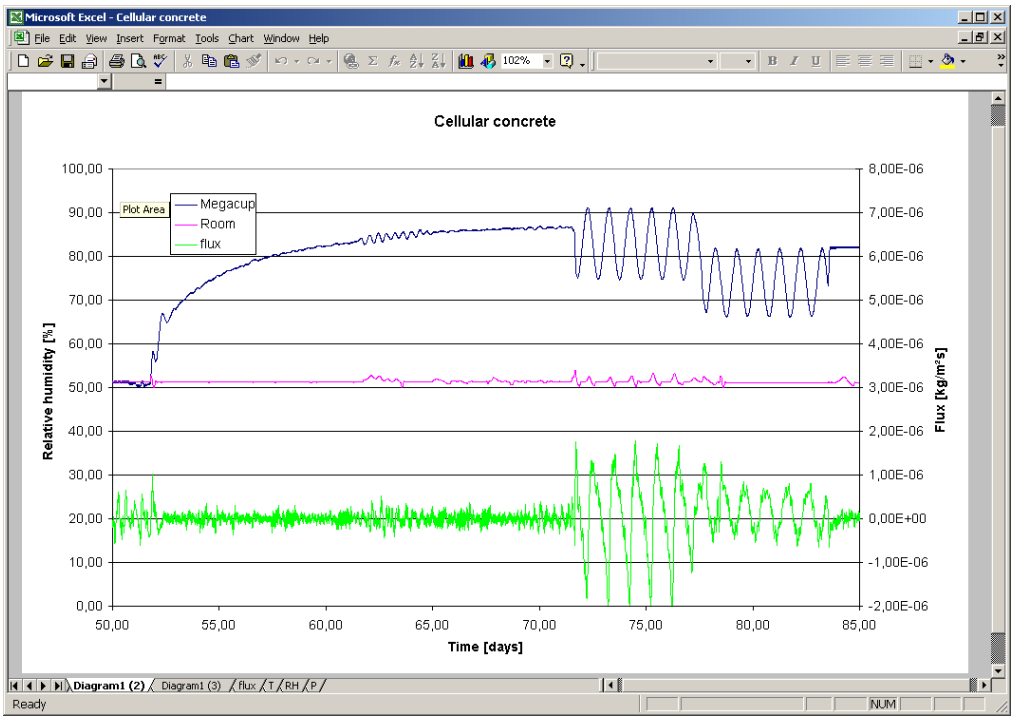

Use of the data

The data can be used to make diagrams that show the variations inside the sample material. An example is the variation of relative humidity, which is shown in the following.

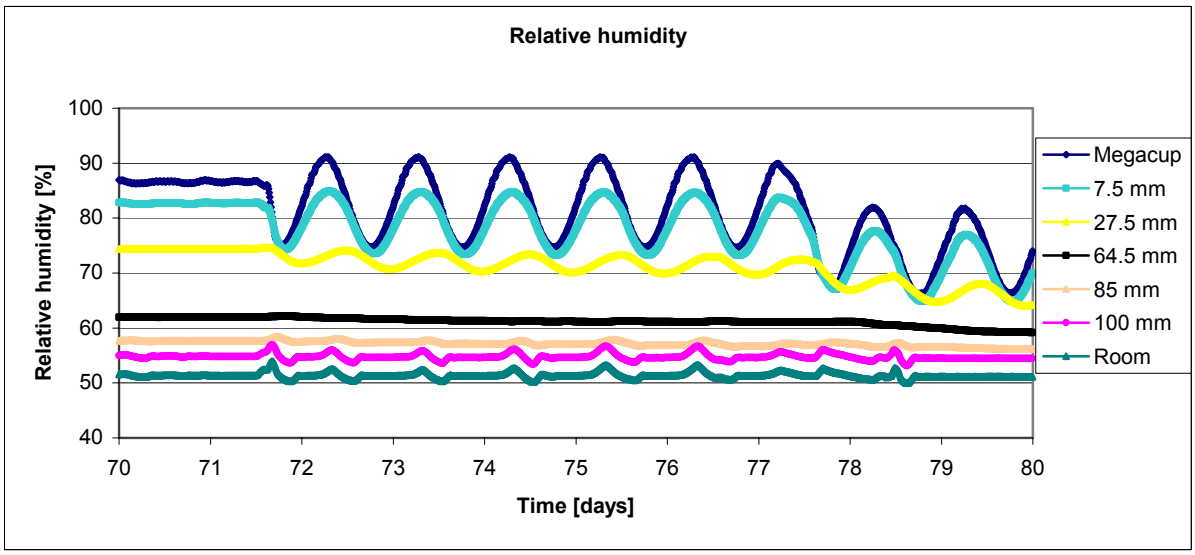

The graph shows the changes in relative humidity through the material sample, which in this case is cellular concrete for a certain period of time.

In the time period between approximately 70 – 71.6 days the boundary condition is for a steady state case 1 (no flux). The next period the boundary condition is dynamic case 2, and from approximately 77.7 days the boundary condition is changed to dynamic case 1.

The changes in boundary condition and time periods without control over the climate in the megacup have to be detected individually for all materials. The tests are not made in a regular order, because time limits caused different orders due to minimizing the time to equilibrium for the different test cases.